

Eindhoven University of Technology

BACHELOR

Fresnel diffraction on a semi-infinite opaque screen

Loenen, S.J.H.

Award date:
2015

Disclaimer

This document contains a student thesis (bachelor's or master's), as authored by a student at Eindhoven University of Technology. Student theses are made available in the TU/e repository upon obtaining the required degree. The grade received is not published on the document as presented in the repository. The required complexity or quality of research of student theses may vary by program, and the required minimum study period may vary in duration.

General rights

Copyright and moral rights for the publications made accessible in the public portal are retained by the authors and/or other copyright owners and it is a condition of accessing publications that users recognise and abide by the legal requirements associated with these rights.

- Users may download and print one copy of any publication from the public portal for the purpose of private study or research.
- You may not further distribute the material or use it for any profit-making activity or commercial gain

Take down policy

If you believe that this document breaches copyright please contact us providing details, and we will remove access to the work immediately and investigate your claim.

Fresnel diffraction on a semi-infinite opaque screen

CQT 2015-06

July 6, 2015

Student: S.J.H. Loenen 0820802
Supervisor: prof. dr. ir. O.J. Luiten
Supervisor: dr. ir. E.D.J. Vredenbregt

Abstract

In the CQT group electron beams are developed to enable for example time-resolved electron diffraction of macromolecular crystals. For electron diffraction to occur at these crystals, the coherence length of the electron beams needs to be larger than the typical length of these crystals. Therefore a method to determine the coherence length of an electron beam is important. One method is based on Fresnel diffraction and has already been used by N. De Jonge[1].

However he described the Fresnel diffraction pattern by a point source, which has an infinitely small waist. It would be more realistic to describe the diffraction pattern by a Gaussian beam. For this reason the Fresnel diffraction theory of a Gaussian beam needs to be known. Up till now it is unknown to the author that this theory is already existent. Therefore in section 2 of this thesis a new theory on Gaussian beam diffraction is developed. The diffraction is on a semi-infinite opaque screen. This has been done by first considering the Fresnel diffraction patterns of a plane wave and a point source, since a Gaussian beam actually is a plane wave or a point source in two different limits. The Gaussian beam describes the entire range from point source to plane wave.

The theory of section 2 has been tested in an experiment. In section 3.1 the experimental setups will be discussed. Herein a HeNe laser emitting a Gaussian beam is shone on a aluminum plate that serves as a semi-infinite opaque screen. The Fresnel diffraction patterns of this Gaussian beam are detected on a CCD camera. Using lens systems a plane wave and a point source are mimicked to also test their diffraction patterns. The results of these experiments are shown in section 4 and verify the theory developed. Testing the theory developed was the extension of my bachelor end thesis and section 4 is completely dedicated to this extension. The influence of different parameters on the position of the diffraction pattern, the fringe spacing and the form of the diffraction pattern are understood. Also the influence of the Gaussian amplitude fall-off in a Gaussian beam is understood. From the experiments it also turned out that lenses used in the setup could influence the diffraction pattern.

At last a short elaboration of the use of Fresnel diffraction in the determination of the degree of coherence of a partially coherent electron beam is given in section 5. In this section the influence of the partial coherent character of a beam on the Fresnel diffraction pattern is shown, which is a blurring of the Fresnel fringes. The blurring causes a decrease in visibility of these fringes and this visibility actually is a measure for the degree of coherence of an electron beam.

Contents

1	Introduction	1
2	Theory of Fresnel diffraction	2
2.1	General Fresnel diffraction	2
2.2	Plane wave diffraction	4
2.3	Point source diffraction	8
2.3.1	Comparison point source diffraction and plane wave diffraction	11
2.4	Derivation field expression gaussian beam	12
2.4.1	Determination expressions $q(z)$ and $P(z)$	13
2.4.2	Complete field expression	14
2.5	Diffraction of a Gaussian beam	15
2.5.1	Diffraction of general Gaussian beam	15
2.5.2	Intensity profile diffracted Gaussian beam - Diffraction form factor . .	16
2.5.3	Intensity profile diffracted Gaussian beam - Gaussian fall-off term . .	18
2.5.4	Off axis Gaussian beam and slit geometry	19
3	Experimental setup	22
3.1	Experimental setup for testing theory on gaussian beam diffraction	22
3.1.1	Beam waist calibration and CCD resolution verification	24
4	Results and Discussion	27
4.1	Plane wave diffraction	27
4.1.1	Plane wave noise correction	27
4.1.2	Analyzing Fresnel diffraction patterns of a plane wave	28
4.2	Plane wave diffraction with a smaller waist	30
4.2.1	Noise correction in plane wave smaller waist setup	31
4.2.2	Analyzing Fresnel diffraction patterns of a plane wave with a smaller waist	33
4.3	Point source diffraction	37
4.3.1	Point source noise correction	37
4.3.2	Analyzing Fresnel diffraction patterns of a point source	38
4.4	Intermediate case diffraction	41
4.4.1	Intermediate case noise correction	41
4.4.2	Analyzing Fresnel diffraction patterns of an intermediate case Gaussian beam	42
5	Fresnel diffraction and coherence of electron beam	44
6	Conclusion	48
6.1	Outlook	48
7	References	50
A	Derivation of relation between errorfunction and fresnelfunction	51

B Derivation expressions Γ and ϕ	51
B.1 derivation of simplified relation for γ	51
B.2 deriving the expression for $\sqrt{\frac{2}{\pi}} \frac{\beta}{2\sqrt{\gamma}}$	52
C Derivation width gaussian beam after diffraction	53
D Beam size measurement	55
E Camera angle influence	56
F Fit parameters of section 4	56

1 Introduction

In the contemporary world, the physics of structures and dynamics at the atomic scale are gaining importance. 3D structures of proteins and other biomolecules are an important source of insight into the function and mechanism of biological processes [2]. To visualize these small scales microscopy techniques need to be used. Optical microscopes using visible light however are not capable of visualizing these atomic structures and dynamics since the spatial resolution is limited by the diffraction limit [3]. Using electron microscopes the diffraction limit can be decreased down to spatial resolutions of sub angströms wherefore individual atoms could be seen [4].

The physical phenomena that serves as the basis to reach this small spatial resolution is electron diffraction. Electron diffraction data of the protein microcrystals lysozyme can be used to determine the 3D structure of this protein microcrystal[2]. Electron diffraction is also used in the structural analysis of atoms. A structural analysis of Si(111) has been conducted using electron diffraction and microscopy by ultrahigh vacuum[5]. Electron diffraction is not only used in the determination of structures of biological molecules and other samples, it is also applied to investigate atomic dynamics on timescales in the femtosecond range[6]. A tantalizing goal of this ultra fast electron diffraction is to map out, in real time, the coordinates of all individual atoms in chemical and biological reactions[7].

So electron diffraction is a useful tool to analyze structures on the nanometer scale and is promising to be used in investigating dynamics on the ultra short time scale. However, for electron diffraction to take place actually, and thus for all the research above to be applicable, the coherence length of the electron beam used for the electron diffraction must exceed the typical length scales of the samples that are investigated. In the UCP setup in the CQT lab an electron beam is created which is partially coherent. This means its coherence length could be smaller than typical length scales of samples that are potentially interesting to analyze. So before experiments on this sample will be done, the coherence length of the electron beam needs to be known.

A method that has been used by N. de Jonge to test this coherence is based on diffraction itself[1]. His electron beam diffracted on a circular hole in a carbon film of a TEM grid and showed a Fresnel diffraction pattern. Fresnel diffraction is the near field diffraction on contrary to Fraunhofer diffraction which is far field diffraction [8]. The pattern measured consisted of diffraction fringes and the number of diffraction fringes that meet a countability criterion is a measure for the coherence. N. De Jonge used a carbon nanotube as source of electrons. This source size in his setup equaled 2.1 nm which allowed him to describe the diffraction pattern by point source diffraction, which is known in literature [9].

The CQT UCP setup the electron beam can be focused to $1 \mu\text{m}$ [10]. With this focus being larger than the source size of N. De Jonge, it is more realistic to describe the diffraction pattern by a beam with a finite waist instead of a point source that has an infinitely small waist. Such a beam with a finite waist is the Gaussian beam and equals a point source in the limit that its waist is made infinitely small. As far as known by the author the Fresnel diffraction pattern of a Gaussian beam is not known. Since the coherence of the CQT UCP setup electron beam can be tested using Fresnel diffraction and that a Gaussian beam is used to describe the electron beam, in this thesis the Fresnel diffraction pattern of a Gaussian beam is investigated.

2 Theory of Fresnel diffraction

2.1 General Fresnel diffraction

In this chapter there will be elaborated on the theory of Fresnel diffraction on a semi-infinite opaque screen. Basically there are two regimes in diffraction theory, Fraunhofer diffraction and Fresnel diffraction [8]. Fraunhofer diffraction is known as the far field diffraction whereas Fresnel diffraction is known as the near field diffraction. The parameter separating Fraunhofer diffraction from Fresnel diffraction is the Fresnel number defined as

$$F = \frac{a}{\sqrt{\lambda r_0}}, \quad (2.1)$$

where a is the width of the aperture whereon diffraction takes place, λ is the wavelength of the incoming wave and r_0 is the distance between the aperture and the plane where the diffraction is measured. This is indicated in Figure 1, where in Figure 1a the aperture size a is small compared with $\sqrt{r_0 \lambda}$ and there is dealt with Fraunhofer diffraction whereas in Figure 1b the aperture is large and there is dealt with Fresnel diffraction. As a rough boundary, Fraunhofer diffraction occurs as the Fresnel number is smaller than one and Fresnel diffraction occurs if the Fresnel number is larger than one [8].

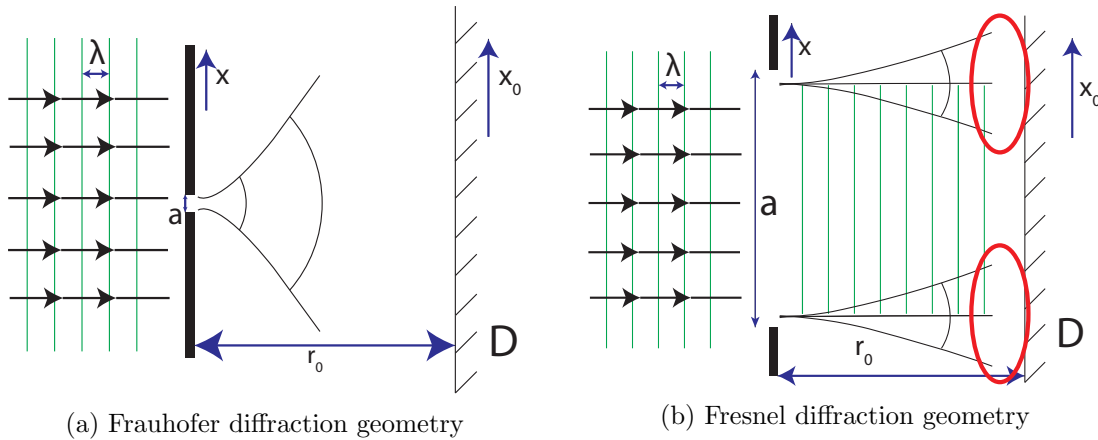


Figure 1: The difference between Fraunhofer and Fresnel diffraction.

What is seen in the Fraunhofer diffraction geometry is a wave falls on the aperture and after the aperture the wave is bended very strong. As a result diffraction effects of the edges are dominated by the bending of the wave and edge effects are not visible. In the Fresnel diffraction case however, the aperture is larger and the wave is not bended as much as in the Fraunhofer diffraction by the aperture. Therefore diffraction effects of the edges are visible, and it is actually this what is Fresnel diffraction: diffraction of the edges.

Diffraction takes place under small angles. As will be shown soon, calculating diffraction patterns involves the integral over the coordinate of the plane of the aperture, indicated by D in Figure 1. Next to that the difference between a point on screen D and a point in the plane of the aperture is important. Since diffraction only takes place at small angles, this distance could be Taylor expanded in terms of the coordinate of the plane of the aperture. This results in the following approximation that is called the Fresnel approximation.

$$r = \sqrt{r_0^2 + (x_0 - x)^2} \approx r_0 + \frac{(x_0 - x)^2}{2r_0} \quad (2.2)$$

In this approximation terms of x^2 occur. In the Fraunhofer diffraction this term is neglected. Mathematically speaking, this approximation is the difference between Fraunhofer and Fresnel diffraction.

In the following Fresnel diffraction patterns of a plane wave, a point source and a Gaussian beam will be derived. A perfect plane wave and a perfect point source actually are ideal wave patterns and are not encountered in nature. The wave pattern that is encountered in nature is a Gaussian beam[11]. In section 2.4.2 it will be shown that in a certain limit, this beam resembles a plane and in another limit it resembles a point source. The Gaussian beam actually covers the entire range from a point source to a plane wave. Here the basic principles of Fresnel diffraction are explained that are valid for an arbitrary wave coming into the plane of the aperture.

In this thesis the Fresnel diffraction on a semi-infinite opaque screen will be considered, as shown in the diffraction setup used in Figure 2. Since the screen is semi-infinite, the width of the aperture is infinite and therefore the Fresnel number is certainly larger than 1 which means Fresnel diffraction occurs in this setup. In the following of this theses $\psi(x, z)$ will be used to describe an electric field.

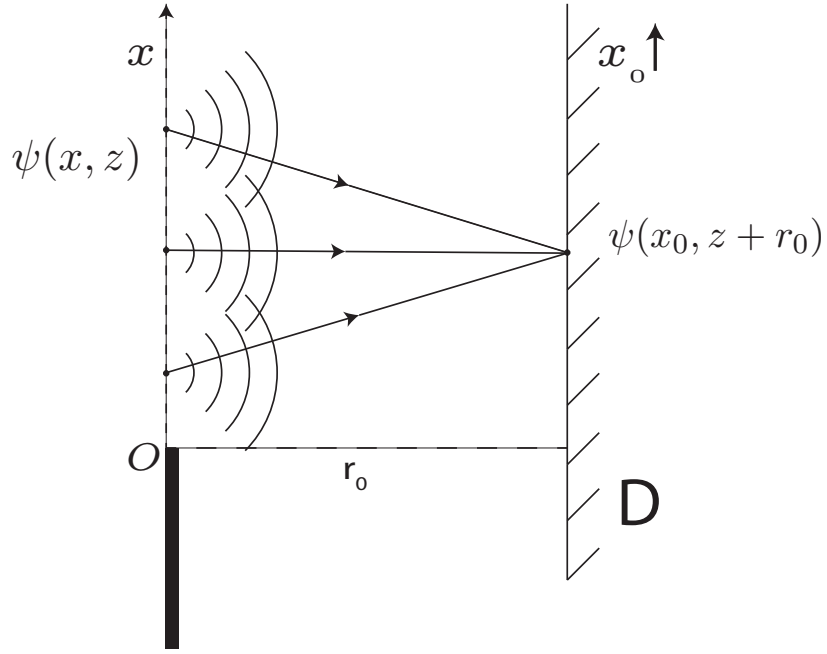


Figure 2: Diffraction setup of Fresnel diffraction on a semi-infinite opaque screen with r_0 the distance between the semi-infinite opaque screen and the screen where the Fresnel diffraction pattern is measured, D . The incoming electric field distribution or wave front is called $\psi(x, z)$.

The electric field distribution at the detector screen D is called $\psi(x_0, z + r_0)$

Basically the only two things necessary to derive Fresnel diffraction is the Huygens-Fresnel principle and the Fresnel approximation in equation (2.2). The Huygens-Fresnel principle states that “every unobstructed point of a wavefront at a given instant in time, serves as a source of spherical secondary wavelets (with the same frequency as that of the primary wave). The amplitude of the optical field at any point beyond is the superposition of all these wavelets (considering their amplitudes and relative phases)”. So what the Huygens-Fresnel principle says for the geometry in Figure 2 is that the optical

field at D is the superposition of secondary spherical wavelets emanating from unobstructed points in the plane of the semi-infinite opaque screen. Three secondary spherical wavelets have been shown in Figure 2 as an illustration. Since at the unobstructed part of the wave front there is an infinite number of infinitely small spaced secondary spherical wavelet, the superposition of these could be translated mathematically into an integral. This means, with a normalization factor in front of the integral, that the wavefront at D can be determined by[9]

$$\psi(x_0, z + r_0) = \frac{1}{i\sqrt{\lambda r_0}} \int_A \Psi(x, z) \exp(ikr) dx, \quad (2.3)$$

where $\Psi(x, z)$ is the incoming wave front, $\psi(x, z)$, multiplied with a transmission function of the semi infinite opaque screen, $O(x, z=0)$. This transmission function takes into account where the wave is unobstructed and therefore from which point secondary spherical wavelets emanate. Since The aperture whereon diffraction takes place here is a semi-infinite opaque screen, the transmission function is 1 above the screens edge and 0 below. So actually the transmission function is a Heaviside step function.

The Fresnel approximation is used in the propagation term of the secondary spherical waves. Therefore r in equation (2.3) is replaced by (2.2). The integral in equation (2.3) runs over the entire plane of the semi-infinite opaque screen. This together with the Heaviside behavior of the transmission function makes the integral over $\psi(x, z)$ run from $x = 0$ till $x = \infty$. Thus the Fresnel diffraction pattern, $\psi(x_0, z + r_0)$, on a semi-infinite opaque screen of any arbitrary wave front can be derived using

$$\psi(x_0, z + r_0) = \frac{1}{i\sqrt{\lambda r_0}} \exp(ikr_0) \int_0^\infty \psi(x, z) \exp\left[\frac{ik}{2r_0} (x - x_0)^2\right] dx. \quad (2.4)$$

2.2 Plane wave diffraction

The Fresnel diffraction behavior of a plane wave that has diffracted on a semi-infinite opaque screen is well known in literature[9] and serves as a first step to analyze the problem of an incident Gaussian beam on a semi-infinite opaque screen. In this section this electric field distribution of a diffracted plane wave will be derived. From this field distribution the intensity, and therefore the diffraction pattern, can be easily derived.

The geometry that is used to describe the Fresnel diffraction of a plane wave is illustrated in Figure 3.

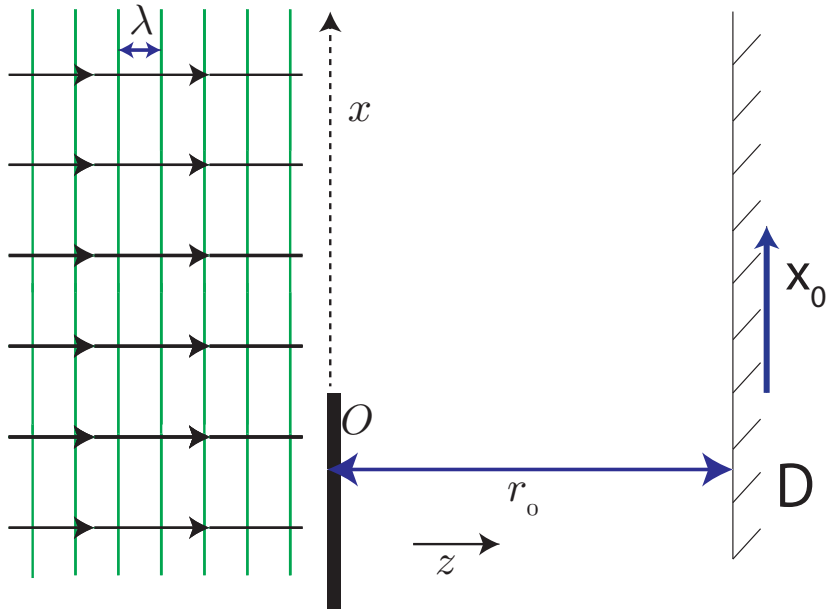


Figure 3: The diffraction geometry of a plane wave with wavelength λ incident on a semi-infinite opaque screen. The distance between the screen and the plane where the diffraction is detected is r_0 .

In this Geometry, x_0 is the vertical distance above the screen's edge in the plane where the electric field, or rather intensity, is measured. This plane is indicated by D . The distance between the semi-infinite opaque screen and D is equal to r_0 . For the wavelength of the light λ is used.

The diffraction pattern of an incident plane wave can be derived using the Huygens-Fresnel principle and the Fresnel approximation as shown in section 2.1. The only thing that still needs to be specified is the incoming wave front, $\psi(x, z)$. In the plane wave case this equals $E_0 \exp(ikz)$, where E_0 is the amplitude of the electric field. Since the concern is on the form of the diffraction pattern and not on the theoretical details concerning the intensity in the following E_0 is set to 1. To derive the Fresnel diffraction pattern of a plane wave, $\psi(x, z) = \exp(ikz)$ is substituted in equation (2.4).

To evaluate this integral, a new dimensionless variables μ is introduced as follows:

$$x = x_0 + L\mu, \quad \text{where} \quad L = \sqrt{\frac{\lambda r_0}{2}}. \quad (2.5)$$

By substituting these relations in equation (2.1) one arrives at

$$\psi(x_0, r_0) = \frac{\exp(ikr_0)}{\sqrt{2i}} \int_{-\frac{x_0}{L}}^{\infty} \exp\left(\frac{i\pi}{2}\mu^2\right) d\mu. \quad (2.6)$$

The integral in equation (2.6) is recognized as a Fresnel integral $F(\theta)$; where $F(\theta) = \int_0^\theta \exp\left(\frac{i\pi}{2}\theta'^2\right) d\theta'$. These Fresnel integrals have been extensively studied, and their numerical values are tabulated [8]. In this report $F(\dots)$ is referred to as the Fresnel function. This Fresnel function is uneven and thus obeys the relation $F(-\theta) = -F(\theta)$. In the limit that $\theta \rightarrow \infty$, $F[\theta] = \frac{1+i}{2}$

Using these properties, and the definition of L , the electric field distribution at D can be derived to be:

$$\psi(x_0, r_0) = \exp(ikr_0) \frac{1}{2} \left[1 + (1-i)F\left(\sqrt{\frac{2}{r_0\lambda}}x_0\right) \right], \quad (2.7)$$

where a constant factor of $(1 - i)$ is omitted that bears no significance since the pattern that will eventually be measured is the absolute value squared of equation (2.7).

To gain a better physical understanding of the diffraction pattern, $F(\theta)$ is approximated by $F(\theta) = \frac{1+i}{2} + \frac{1}{i\pi\theta} \exp\left(\frac{i\pi}{2}\theta^2\right)$. This approximation is valid only when $\theta \gg 1$, but turns out to be already very accurate for $\theta = 2$ [9]. Using this approximation the field distribution in (2.7) becomes

$$\psi(x_0, r_0) = \exp(ikr_0) \left[1 - \frac{\sqrt{r_0\lambda}}{2\pi x_0} \exp\left(\frac{i\pi}{4}\right) \exp\left(\frac{i\pi}{r_0\lambda}x_0^2\right) \right]. \quad (2.8)$$

This equation describes the field distribution, and therefore the interference pattern of a plane wave diffracting on a semi-infinite opaque screen. Equation (2.8) shows that the diffraction pattern arises from the interference between a plane wave propagating as if there was no screen, represented by the $\exp(ikr_0)$, and a virtual wave which phase information resembles a cylindrical wave[8] and decreases in amplitude with vertical distance as $\frac{1}{x_0}$, represented by the second term in the brackets of (2.8). This virtual cylindrical wave emanates from the edge of the semi-infinite opaque screen, as is shown in Figure 4.

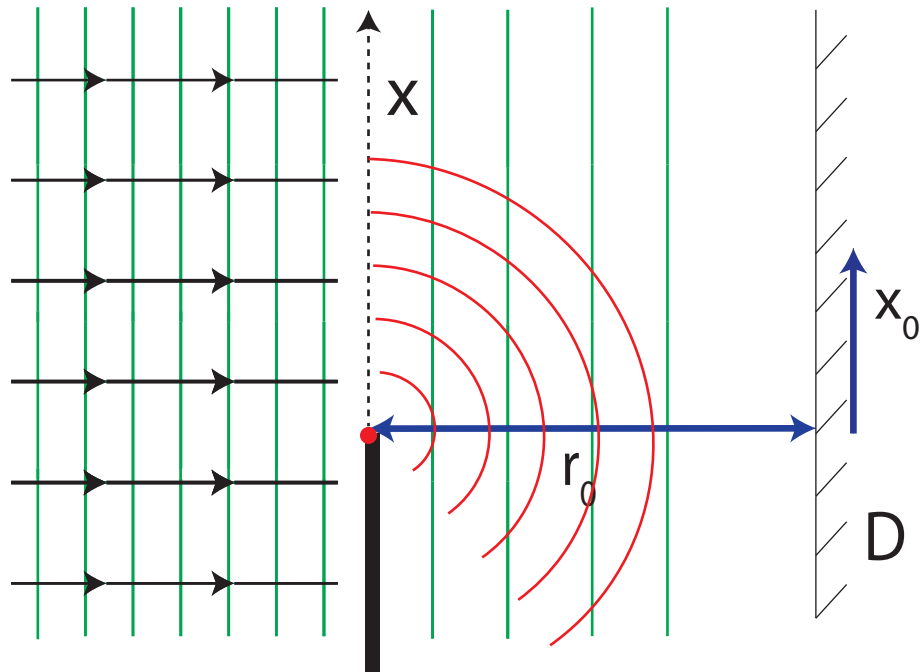


Figure 4: visualization of the interference between the point source and the cylindrical wave that emanates from a virtual point indicated by the red dot.

The amplitude of the virtual cylindrical wave falls off as $\frac{\sqrt{r_0\lambda}}{2\pi x_0}$. After multiplication by $\frac{r_0}{r_0}$ and using that $\alpha = \frac{x_0}{r_0}$, this equals $\sqrt{\frac{\lambda}{r_0}} \frac{1}{2\pi\alpha}$. So looking at the same angle, but at different distances from the semi-infinite opaque screen(r_0), the influence of this term falls off as $\sqrt{\frac{1}{r_0}}$, which is similar to the distance dependence of a cylindrical wave[8]. Next to that the amplitude factor decreases for increasing α , when r_0 is fixed. This could be understood by the fact that a larger α means more distance to travel for the wave emanating from the screens edge, which therefore decreases in intensity based on an argument concerning energy conservation. So in the interference with the plane wave, the plane wave will become more

dominant with increasing α .

From (2.8) the intensity distribution and therefore a measurable diffraction pattern can be derived. Using that the intensity scales as the absolute value squared of the field distribution, so $I \propto \psi^*(x_0, r_0)\psi(x_0, r_0)$, the intensity distribution becomes

$$I(x_0, r_0) \approx \left[1 - \frac{\sqrt{r_0 \lambda}}{\pi x_0} \cos \left(\frac{\pi}{2} \left[\frac{2x_0^2}{\lambda r_0} + \frac{1}{2} \right] \right) \right], \quad (2.9)$$

where terms of order $O(\theta^{-2})$ are neglected. This is valid since the electric field distribution of equation (2.8) is derived under the condition that $\theta \gg 1$.

If the cosines term in the expression above reaches one of its extreme values a (local) maximum or minimum will occur in the diffraction pattern. This gives for the position of the local maxima and minima of the intensity pattern that

$$x_{0,n\max} = \sqrt{\lambda r_0 \left(2n + \frac{3}{4} \right)} \quad (2.10a) \quad x_{0,n\min} = \sqrt{\lambda r_0 \left(2n - \frac{1}{4} \right)} \quad (2.10b)$$

with $x_{0,n}$ in equation (2.10a) for the positions of the maxima and in equation (2.10b) for the positions of the minima. In these equations n is a positive integer, with $n \geq 1$.

This derivation could easily be extended to a 3D situation where the y -direction is taken into account. However since a plane wave and the semi-infinite opaque screen are symmetric in the y -direction, the diffraction pattern is independent on y .

In Figure 5 the analytical Fresnel diffraction pattern is plotted. This is the absolute square of equation (2.7) with θ as argument of the Fresnel function instead of $\frac{x_0}{L}$. What Figure 5 shows is that the diffraction pattern has fringes that decrease in amplitude as the argument of the Fresnel function increases. Also the fringe spacing decreases as this argument increases, which is stated in equation (2.10).

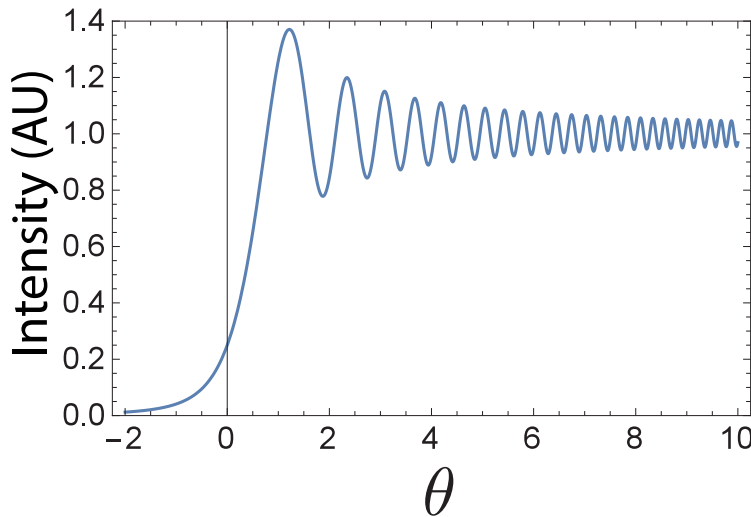


Figure 5: the Fresnel diffraction pattern of plane wave, which is intensity pattern generated by the electric field of (2.7)

It is convenient to define a region wherein the diffraction fringes are clearly visible and where they are not. In this report it shall be used that the diffraction pattern is clearly visible when $-1 \leq \theta \leq 10$. So the region where diffraction fringes are clearly visible is defined by

$$-\sqrt{\frac{r_0\lambda}{2}} \leq x_0 \leq 10\sqrt{\frac{r_0\lambda}{2}}. \quad (2.11)$$

The reason why the diffraction pattern decreases as θ increase because the influence of the cylindrical wave in the diffraction pattern decreases linearly with θ and therefore linearly with distance x_0 .

2.3 Point source diffraction

Where a plane wave is infinitely extended and has no divergence, a point source is infinitely small and has an infinite divergence. As mentioned in section 2.1 the point source, as well as the plane wave, are ideal sources. In this section the Fresnel diffraction pattern of a point source will be derived since it gives insight in the Fresnel diffraction pattern of a Gaussian beam. The derivation is based on the one executed in Wave Optics [9]. The description of the diffraction pattern will be done using Figure 6.

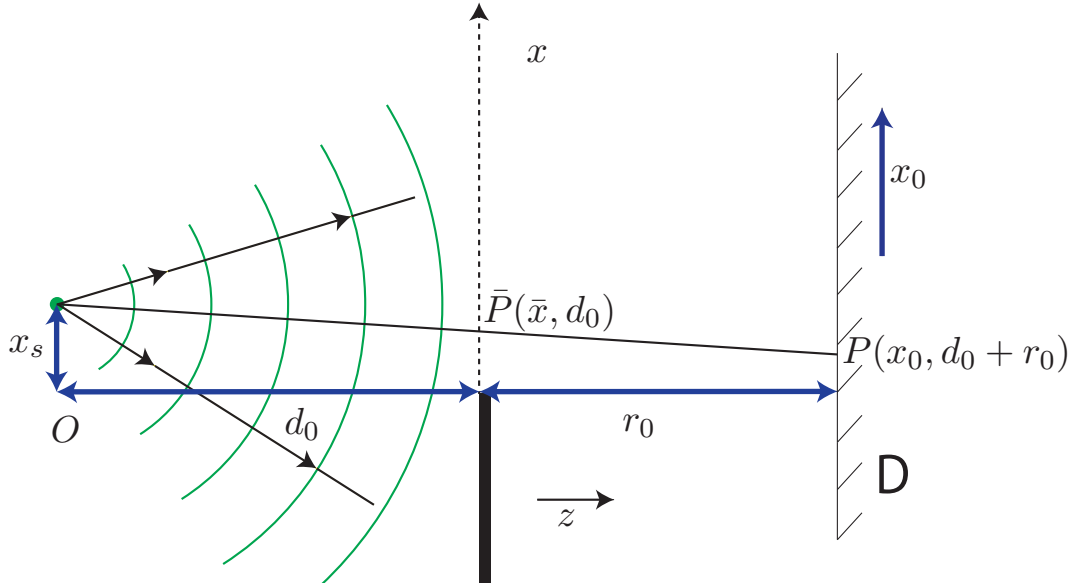


Figure 6: visualization on how to describe the Fresnel diffraction pattern of a spherical point source.

In Figure 6 Q represents a point source that emits a spherical wave is positioned at $(x_s, 0)$. The horizontal distance between Q and the semi-infinite opaque screen is d_0 , and the horizontal distance of the semi-infinite opaque screen to the detector screen is r_0 . The height of the point source compared to the screens edge is indicated by x_s .

Again the framework derived in section 2.1 is used to determine the Fresnel diffraction pattern. The derivation will be done in 2D, and could easily be extended to 3D. A 2D point source actually is a cylindrical wave. Therefore, in case of a 2D point source, the incoming wave is not planar as in the plane wave case, but is circular. The electric field distribution, $\psi(x, d_0)$, of the incoming wave then is

$$\psi(x, d_0) = \frac{1}{\sqrt{d_0}} \exp(i k d_0) \exp\left[\frac{ik}{2d_0}(x - x_s)^2\right], \quad (2.12)$$

which is the paraxial approximation of the electric field of a point source. The paraxial approximation is allowed since in Fresnel approximation it is also assumed that angles are small. Basically this paraxial approximation is equivalent to the Fresnel approximation. Substituting this electric field distribution in the integral of equation (2.4), the integral could be rewritten to a more convenient form where

$$\psi(\bar{x}, d_0 + r_0) = \frac{1}{i\sqrt{\lambda d_0 r_0}} \exp(ikD) \int_0^\infty \exp\left[\frac{ik}{2f}(x - \bar{x})^2\right] dx. \quad (2.13)$$

Here D is the Fresnel approximated distance between the point source, $(x_s, 0)$, and a point on the detector screen, $(x_0, d_0 + r_0)$. Next to D two other new variables are introduced, f and \bar{x} , and are defined as

$$\frac{1}{f} = \frac{1}{d_0} + \frac{1}{r_0}, \quad \bar{x} = \frac{d_0 x_0 + r_0 x_s}{d_0 + r_0}. \quad (2.14)$$

In deriving equation (2.13) from the integral of equation (2.4) terms of $(x - \bar{x})^2$ are separated from terms of $(x_0 - x_s)^2$. This automatically brings in the new parameter f , but also allows to conveniently introduce a dimensionless variable ν that is used to evaluate the integral of equation (2.13). The variable μ is introduced as

$$x = \bar{x} + L' \nu, \quad \text{where} \quad L' = \sqrt{\frac{\lambda f}{2}}. \quad (2.15)$$

From this point on the further derivation is mathematically completely identical to the derivation of the plane wave Fresnel diffraction pattern. The only difference is the name of the parameters; in the point source case \bar{x} is used instead of x_0 and f is used instead of r_0 . Therefore it is allowed to use the same mathematical results as in the plane wave Fresnel diffraction. In the plane wave case the exact expression of the electric field distribution at the detector screen has been derived as well as an approximation that is valid when the argument of the Fresnel function is larger than one. By doing this approximation the spacing between fringes had been derived based on the intensity distribution of the diffracted plane wave. For the point source Fresnel diffraction this will also be done.

By changing f for r_0 and \bar{x} for x_0 in equation (2.7) the exact, where here exact is meant in the Fresnel approximation, electric field distribution of the point source diffraction equals

$$\psi(x_0, d_0 + r_0) = \frac{1}{\sqrt{d_0 + r_0}} \exp(ikD) \frac{1}{2} \left[1 + (1 - i)F\left(\sqrt{\frac{2}{f\lambda}}\bar{x}\right) \right]. \quad (2.16)$$

Then by using the approximation of the Fresnel function the electric field distribution becomes

$$\psi(\bar{x}, d_0 + r_0) = \frac{1}{\sqrt{d_0 + r_0}} \exp(ikD) \left[1 - \frac{\sqrt{f\lambda}}{2\pi\bar{x}} \exp\left(\frac{i\pi}{4}\right) \exp\left(\frac{i\pi}{f\lambda}\bar{x}^2\right) \right]. \quad (2.17)$$

As in the plane wave case, the resulting diffraction pattern is the interference between the incoming wave, a point source/cylindrical wave here, and a wave that resembles a cylindrical wave. Notice however that in the plane wave case the cylindrical wave emanated from the screens edge with $x_0 = 0$ a distance r_0 in front of the detection screen. Here the cylindrical wave emanates from $\bar{x} = 0$ which gives $x_0 = \frac{r_0}{d_0}x_s$ and is a distance f in front of the detector screen instead of r_0 . This is shown in Figure 7 below.

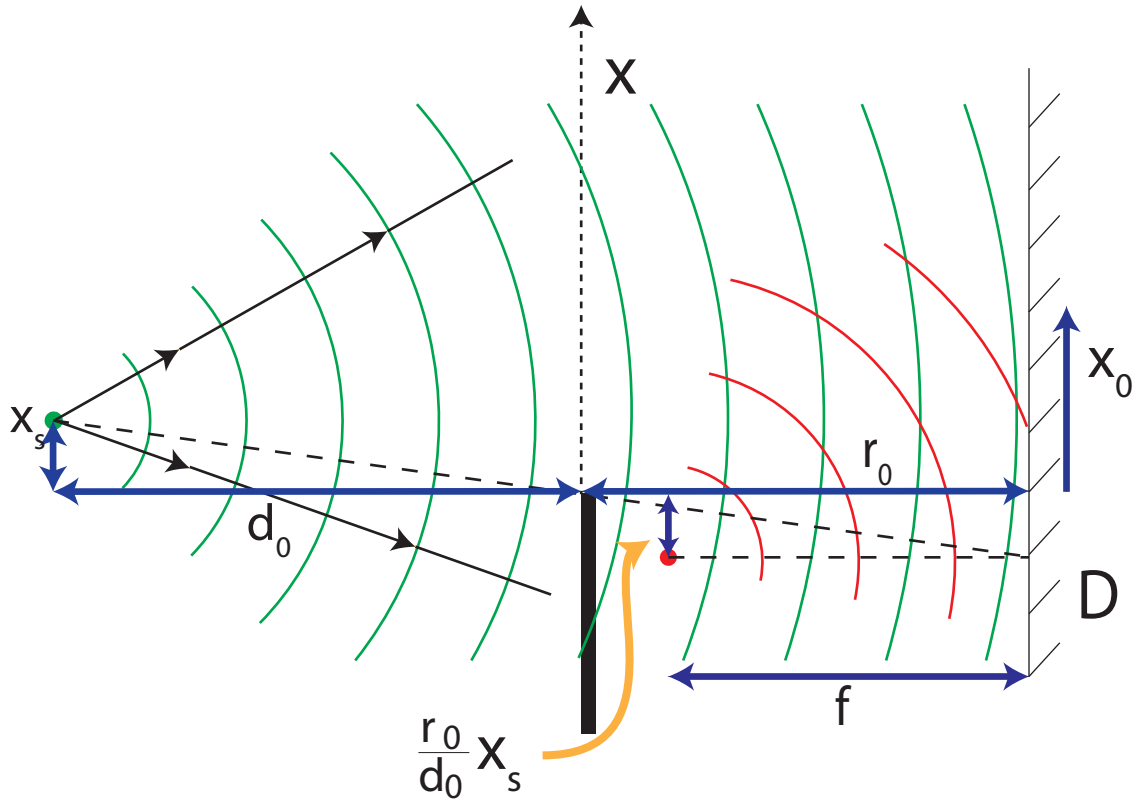


Figure 7: visualization of the interference between the point source and the cylindrical wave that emanates from a virtual point indicated by the red dot

What is seen from Figure 7 is that the virtual point where from the cylindrical wave is emitted is shifted downwards by an amount of $\frac{r_0}{d_0} x_s$ if x_s is shifted upwards.

The shifting effect of x_s is shown in Figure 8, where the diffraction patterns are shown of two point sources/cylindrical waves. The values of the parameters of the two figures are shown in Table 1. To visualize the effect of x_s an offset has been added to the orange diffraction patterns. Notice the only difference is x_s and only a shifting has occurred in the opposite direction as x_s has shifted relatively to the screens edge.

Table 1: Parameters of diffraction pattern in Figure 8

Relevant parameter	Value
$r_0(\text{mm})$	400
$d_0(\text{mm})$	200
x_s orange pattern (μm)	0
x_s blue pattern (μm)	-121
$\lambda(\text{nm})$	632.8

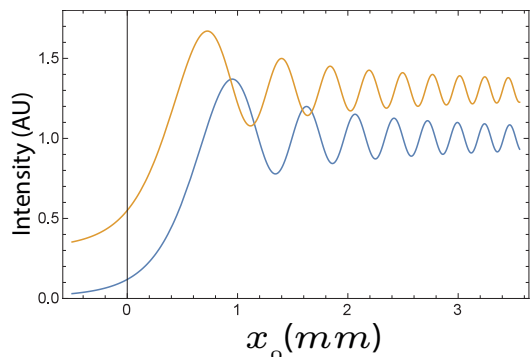


Figure 8: Diffraction pattern of a centered point source (orange) and an off axis point source (blue)

To determine the fringe spacing, the absolute value squared of equation (2.17) is calculated. Thereafter the fringe spacing is derived in the same way as in the plane wave case. This means determining the extreme values of the cosinus term in equation (2.9) with r_0 replaced by f and x_0 replaced by \bar{x} . To express the positions on the detector of the fringes, the positions need to be described by the coordinate on the detector screen, x_0 . This is done by applying the definition of \bar{x} in equation (2.14). This leaves

$$x_{0_{max}} = \frac{d_0 + r_0}{d_0} \sqrt{f\lambda \left(2n + \frac{3}{4}\right)} - \frac{r_0}{d_0} x_s \quad (2.18a)$$

$$x_{0_{min}} = \frac{d_0 + r_0}{d_0} \sqrt{f\lambda \left(2n - \frac{1}{4}\right)} - \frac{r_0}{d_0} x_s. \quad (2.18b)$$

The range where on diffraction takes place can also be determined now by using the criterion that θ in $F[\theta]$ needs to be larger than -1 and smaller than 10. In the point source case $\theta = \sqrt{\frac{2}{f\lambda}}\bar{x}$, thus the diffraction range is

$$-\sqrt{\lambda \frac{r_0(d_0 + r_0)}{2d_0}} - \frac{r_0}{d_0} x_s \leq x_0 \leq 10\sqrt{\lambda \frac{r_0(d_0 + r_0)}{2d_0}} - \frac{r_0}{d_0} x_s. \quad (2.19)$$

where the definition of \bar{x} in terms of x_0 and x_s has been used to describe the range by the parameter of the detector screen, x_0 . From equation (2.19) it is also verified that x_s just shifts the pattern upwards or downwards by a factor $\frac{r_0}{d_0}$ depending on the sign of x_s .

In the plane wave there was a symmetry in the wave front and in the semi-infinite opaque screen in the y -direction. As a result the diffraction pattern was y -independent. A point source has a spherical symmetric wave front and it could be derived that the Fresnel diffraction of a point source is also y -symmetric.

2.3.1 Comparison point source diffraction and plane wave diffraction

The description of the point source Fresnel diffraction has appeared to be mathematically equivalent to the plane waves description. This similarity could be drawn even further. In the limit that a point source is situated infinitely large in front of the semi-infinite opaque screen, so d_0 equal to infinity, the point source resembles a plane wave. This could be understood as the radius of the wave front at the plane of the semi-infinite opaque screen is infinite and therefore the wave front seems planar in this plane of the screen. This means that physically a point source with an infinite d_0 is equivalent to a plane wave. Therefore in this limit the diffraction patterns also need to be equivalent.

The electric field on the detector screen after Fresnel diffraction is described by equation (2.7) for the plane wave and by equation (2.16) for the point source. On behalf of clarity, these electric field expressions are repeated below.

$$\psi(x_0, r_0) = \exp(ikr_0) \frac{1}{2} \left[1 + (1 - i)F\left(\sqrt{\frac{2}{r_0\lambda}}x_0\right) \right]. \quad (2.7)$$

$$\psi(x_0, d_0 + r_0) = \frac{1}{d_0 + r_0} \exp(ikD) \frac{1}{2} \left[1 + (1 - i)F\left(\sqrt{\frac{2}{f\lambda}}\bar{x}\right) \right]. \quad (2.16)$$

Since the measured diffraction pattern is the absolute value squared of these electric field distributions and since amplitude terms are not important for the form of the diffraction pattern, to proof the equivalence the arguments of the Fresnel function need to be equivalent. Evaluating the argument of the Fresnel function in equation (2.16) in the limit that d_0 is infinity gives

$$\lim_{d_0 \rightarrow \infty} \sqrt{\frac{2}{f\lambda}} \bar{x} = \lim_{d_0 \rightarrow \infty} \sqrt{\frac{2}{\lambda}} \sqrt{\left(\frac{1}{d_0} + \frac{1}{r_0}\right) \frac{d_0 x_0 + r_0 x_s}{d_0 + r_0}} = \sqrt{\frac{2}{r_0 \lambda}} x_0, \quad (2.20)$$

which is the argument of the Fresnel function in the plane wave case, equation (2.7), and therefore the equivalence is proven.

2.4 Derivation field expression gaussian beam

In subsection 2.2 and subsection 2.3, the Fresnel diffraction pattern for a plane wave and a point source respectively have been derived. A plane wave has an infinite waist and zero divergence where a point source has the opposite. In reality however, these beam profiles do not occur. A beam profile that does occur in reality is the profile of a Gaussian beam [11]. For this reason Gaussian beams are interesting to analyze.

In this subsection the field expression for the Gaussian beam will be derived. This can be done by using a plane wave expansion that results in a Gaussian beam [12]. One other way is to solve the wave equation, equation (2.21). In this section the latter proposed way will be applied. In subsection 2.5 the diffraction pattern of a Gaussian beam will be investigated and will be compared to the plane wave and point source diffraction.

Since the main interest is in wave fields that vary slowly in the longitudinal direction compared to the transversal direction, wave amplitudes in the paraxial limit will be investigated. Electromagnetic fields in free space are governed in general by the scalar wave equation [11]

$$[\nabla^2 + k^2] \psi(x, y, z) = 0, \quad (2.21)$$

where $\psi(x, y, z)$ is the electric field distribution.

As mentioned, variations of the electric field in the longitudinal direction, z -direction, are small compared to variations in transversal directions. Therefore it is convenient to write the electric field distribution as a product of the propagation factor and a complex scalar wave amplitude which describes the transverse beam profile. Thus as $\psi(x, y, z) = \exp(ikz)\tilde{u}(x, y, z)$, with $\exp(ikz)$ the propagation factor and $\tilde{u}(x, y, z)$ the complex scalar wave amplitude.

By substituting this in equation (2.21), this yields

$$\frac{\partial^2 \tilde{u}}{\partial x^2} + \frac{\partial^2 \tilde{u}}{\partial y^2} + 2ik \frac{\partial \tilde{u}}{\partial z} = 0. \quad (2.22)$$

Here it has been used that $|\frac{\partial^2 \tilde{u}}{\partial z^2}| \ll |2k \frac{\partial \tilde{u}}{\partial z}|, |\frac{\partial^2 \tilde{u}}{\partial x^2}|$ and $|\frac{\partial^2 \tilde{u}}{\partial y^2}|$, which is the mathematical translation that variations in the longitudinal direction are much smaller than variations in the transverse directions. Equation (2.22) shows that there are only second partial derivatives to x and y . This symmetry results in an equivalent dependence of $\tilde{u}(x, y, z)$ on x and y . For this reason, in the following only the x -direction is considered.

The differential equation in equation (2.22) has a form similar to the time-dependent Schrödinger equation. It is easy to see that a solution could be

$$\tilde{u}(x, y, z) = \exp\left(i \left[P(z) + \frac{k}{2q(z)} x^2\right]\right). \quad (2.23)$$

Here $P(z)$ represents the complex phase shift which is associated with the propagation of the beam and $q(z)$ is a complex beam parameter that describes the Gaussian profile and the curvature of the phase front of the beam at a certain distance from the center of the beam [13]. Substituting (2.23) in (2.22) and comparing equal powers of x and y yields

$$q'(z) = 1 \quad P'(z) = \frac{i}{2q(z)}, \quad (2.24)$$

where the primes indicate derivatives to z .

2.4.1 Determination expressions $q(z)$ and $P(z)$

The further derivation is based on an article by Kogelnik and Li [13].

Integrating $q'(z)$ gives $q(z) = z + q_0$. To arrive at a form wherein the amplitude falls off like a Gaussian and where there is a transversal phase variation over a certain area, two real beam parameters, $R(z)$ and $w(z)$, are introduced and are related to $q(z)$ as follows

$$\frac{1}{q(z)} = \frac{i\lambda}{\pi w^2(z)} + \frac{1}{R(z)}. \quad (2.25)$$

The physical meaning of $R(z)$ and $w(z)$ becomes immediately clear as equation (2.25) is substituted in equation (2.23). By doing this it is clear that $R(z)$ is the radius of curvature of the wave front and $w(z)$ is a measure of the decrease in amplitude of the electric field. This decrease in amplitude is Gaussian.

In the beam waist of a Gaussian beam, the position where $z = 0$, the waist is minimal and the wavefront is planar, so $w(0) = w_0$ and $R(0) = \infty$. Using this and equation (2.25) defines $q(0)$ as $q_0 = q(0) = -\frac{i\pi w_0^2}{\lambda}$. So the complex beam parameter is purely imaginary in the beam waist. Substituting this in $q(z) = z + q_0$ gives

$$q(z) = z - i \frac{\pi w_0^2}{\lambda}. \quad (2.26)$$

By comparing the real and imaginary parts of equation (2.25) and equation (2.26) the expressions of w and R could be derived. After a short calculation one obtains

$$w(z) = w_0 \sqrt{1 + \left(\frac{z\lambda}{\pi w_0^2} \right)^2} \quad (2.27a)$$

$$R(z) = z \left[1 + \left(\frac{\pi w_0^2}{z\lambda} \right)^2 \right]. \quad (2.27b)$$

Using these relations, $q(z)$ in equation (2.23) is fully quantified.

Using the expression for $q(z)$ in equation (2.26) and the relation between $P'(z)$ and $q(z)$ in equation (2.24), the expression for $P(z)$ could be obtained by integrating over z . This yields that

$$iP(z) = \ln \left(\sqrt{\frac{w_0}{w(z)}} \right) - \frac{i}{2} \arctan \left(\frac{\lambda z}{\pi w_0^2} \right). \quad (2.28)$$

2.4.2 Complete field expression

Since the expressions of $q(z)$ and $P(z)$ are known, it is possible to construct the field amplitude of a Gaussian beam. Substituting the expressions of (2.28) and (2.25) in equation (2.23) the complex scalar wave amplitude could be written as

$$\tilde{u}(x, z) = \sqrt{\frac{w_0}{w(z)}} \exp\left(-\frac{i}{2} \arctan\left[\frac{\lambda z}{\pi w_0^2}\right]\right) \exp\left(-\frac{x^2}{w^2(z)} + ik \frac{x^2}{R(z)}\right), \quad (2.29)$$

This field expression shows there is a phase shift in the beam waist, $z = 0$, as is represented by the arctan term with the knowledge that it is point symmetric and $\arctan(\infty) = \frac{\pi}{2}$. This phase shift is the famous “Gouy-phase shift” [11].

In Figure 9 the geometry of the Gaussian beam is shown. Here w_0 is the waist of the beam.

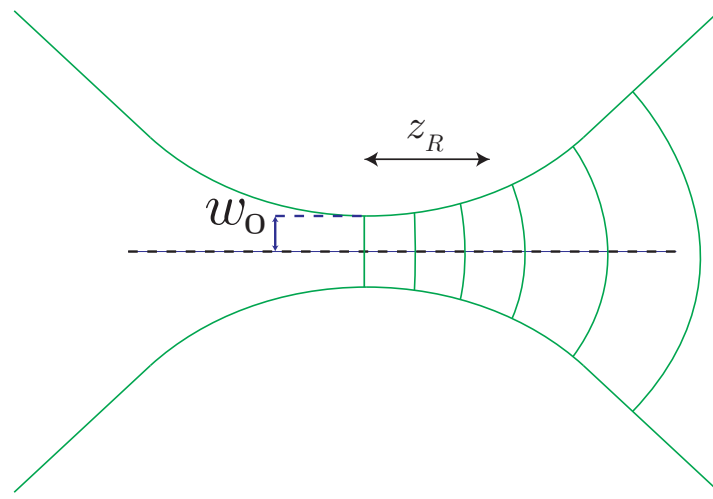


Figure 9: Geometry of a gaussian beam. Far inside the Rayleigh length the wave front is planar, far outside the Rayleigh length, the wave front is circular.

The other parameter next to w_0 shown in Figure 9 is z_R . This parameter is called the Rayleigh length and is defined as [11]

$$z_R = \frac{\pi w_0^2}{\lambda}, \quad (2.30)$$

and defines the region of transition from a planar wave front to a circular wavefront as is shown in Figure 9. By looking at equations (2.27a) and (2.27b), it can be seen that the Rayleigh length is important for the beam width as well as the wave front of the beam. Far inside the Rayleigh length, so close to the waist of the beam, the wave front is planar. This means that in this region, the Gaussian beam resembles a plane wave except for the fact that it has a finite waist. Far outside the Rayleigh length the wave front is circular and therefore the Gaussian beam resembles a point source, again with a finite waist.

In the neighborhood of z_R the wave front is nor planar nor circular but elliptical. This essentially is the region where one could expect differences in the diffraction patterns as compared to the plane wave and the point source. The regime where the wave front is elliptical is called the intermediate case in this thesis since it is in between the plane wave and the point source resemblance of the Gaussian beam.

Returning to the symmetry of x and y in equation (2.22) and the knowledge of the Gaussian

beam profile in the x -direction it can be concluded that the beam profile in the y -direction is equivalent. Thus there is a azimuthal symmetry in the geometry of a Gaussian beam.

2.5 Diffraction of a Gaussian beam

In the previous section the field expression of the Gaussian beam has been derived. Using the Rayleigh length, two limiting cases have been considered for a Gaussian beam; the plane wave and the point source. From these two limiting cases, the Fresnel diffraction pattern is known. The Fresnel diffraction pattern of a Gaussian beam, that is not in its plane wave or point source limit, is unknown. It is therefore interesting that in this section new theory on the Fresnel diffraction pattern of a Gaussian beam is presented. At the end of this section a comparison will be made between the Gaussian beam diffraction pattern and that of a plane wave as well as that of a point source. In the limiting values these diffraction patterns need to be equivalent.

2.5.1 Diffraction of general Gaussian beam

For the derivation of the Fresnel diffraction pattern of a Gaussian beam the framework derived in section 2.1 is applied. The geometry of the Fresnel diffraction is shown in Figure 10, where the origin of the coordinate system is at the beam waist and the distance between the waist and the semi-infinite opaque screen is d_0 . The height of the center of the Gaussian beam is indicated by x_s , but in the upcoming derivation it is assumed that the middle of the beam waist is exactly at the same height as the edge of the semi-infinite opaque screen. So $x_s = 0$. At the end of this section the case of $x_s \neq 0$ will be discussed.

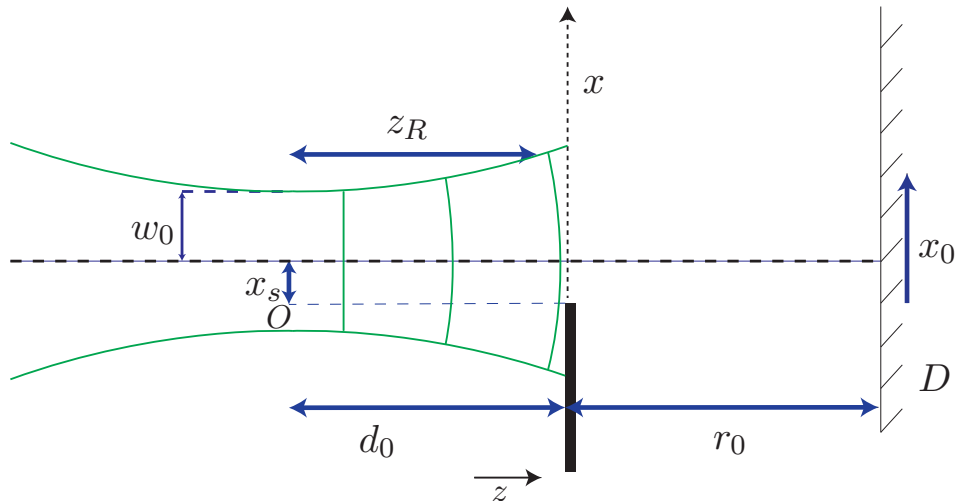


Figure 10: Geometry of Gaussian beam diffraction on a semi-infinite opaque screen. The center of the Gaussian beam is at a height x_s compared to the height of the screen's edge.

In case of Gaussian beam Fresnel diffraction the incoming wavefront $\psi(x, z)$ that has to be substituted in equation (2.4) is the derived Gaussian electric field distribution of equation (2.29). Since the diffraction pattern that is eventually measured is the absolute value squared of the electric field, constant (complex) amplitude terms are disregarded in the derivation since they do not influence the form of the Fresnel diffraction pattern. By doing the substitution just mentioned and defining

$$\gamma = \frac{1}{w_x^2(z)} - \left[\frac{ik}{2R_x(z)} + \frac{ik}{2r_0} \right], \quad (2.31)$$

and

$$\beta = -\frac{ik}{r_0}, \quad (2.32)$$

the integral of (2.4) is evaluated to be

$$\psi(x_0, d_0 + r_0) \propto \exp\left(\frac{\beta^2}{4\gamma}x_0^2\right) \left[1 + \operatorname{erf}\left(\frac{\beta}{2\sqrt{\gamma}}x_0\right)\right] \quad (2.33)$$

where an error function is encountered. As mentioned, the plane wave and the point-source are limiting cases of the Gaussian beam. What is to be noticed is that the expressions of the diffraction patterns of the plane wave and the point source have a factor $[1 + (1 - i)F[\dots]]$, where the Gaussian beam has a factor $[1 + \operatorname{erf}[\dots]]$. Since these expressions determine the form of the interference, and thus diffraction, these factors need to be similar in the limiting cases. This indicates there exist a relation between $F[x]$ and $\operatorname{erf}[x]$. In appendix A a derivation is shown proving

$$\operatorname{erf}[x] = (1 - i)F\left[\frac{2}{\sqrt{\pi}(1 - i)}x\right]. \quad (2.34)$$

From this point on the expression on the right hand side of equation (2.34) will be used instead of $\operatorname{erf}[\dots]$.

2.5.2 Intensity profile diffracted Gaussian beam - Diffraction form factor

Since not the electric field is measured but the intensity, the Fresnel diffraction pattern of a Gaussian beam is proportional to the absolute value squared of equation (2.33). Using the relation between the error function and the Fresnel function the Fresnel diffraction pattern of a Gaussian beam is described by

$$|\psi(x_0, y_0, r_0 + d_0)|^2 = \underbrace{\left| \exp\left(\frac{\beta^2}{4\gamma}x_0^2\right) \right|^2}_{\text{Gaussian fall-off}} \underbrace{\left[1 + (1 - i)F\left[\frac{2}{\sqrt{\pi}(1 - i)}\frac{\beta}{2\sqrt{\gamma}}x_0\right]\right]^2}_{\text{diffraction form factor}}, \quad (2.35)$$

which is the product of a Gaussian fall-off term and a diffraction form factor. The Gaussian fall-off term only describes an amplitude effect, the diffraction form factor however contains the Fresnel function and therefore the information of the fringes in Fresnel diffraction.

In this subsection more is elaborated on the characteristics of the diffraction form factor whereas in the next subsection an elaboration is given on the Gaussian fall-off term.

In the plane wave case as well as in the point source case the argument of the Fresnel function was a real number. However, since γ and β are complex numbers, the argument of the Fresnel function in the diffraction form factor will in general be complex. In the limiting cases of the plane wave and point source the argument thus obviously needs to be real.

The goal will be to express this argument in polar coordinates for the following two reasons; 1) the absolute value of this argument determines the position and spacing of the Fresnel diffraction fringes and 2) the phase of this argument determines the actual shape of the fringes in the Fresnel diffraction pattern.

Physically it is convenient to describe problems dimensionless and this reduces the number of parameters by one since all the relevant parameters as shown in Figure 10 can be described in terms of λ . Doing this leads to the following definitions:

$$\begin{aligned} w_{0x} &= \sigma\lambda \\ z &= \rho\lambda \\ r_0 &= \mu\lambda \\ x_0 &= M\lambda. \end{aligned} \tag{2.36}$$

With this, the argument in the Fresnel function of the diffraction form factor equals,

$$\frac{2}{\sqrt{\pi}(1-i)} \frac{\beta}{2\sqrt{\gamma}} = \pm \frac{1}{\lambda\sqrt{\Gamma}} \exp\left(-\frac{i}{2}\left[\phi + \frac{\pi}{2}\right]\right), \tag{2.37}$$

where the “+” version of this expression is the physically relevant situation. This is shown in appendix B. Would the “−” version be taken, the semi-infinite opaque screen would seem to be upside down. In equation (2.37), Γ is the absolute value of the argument and ϕ determines the phase of the argument. These parameters are derived, see appendix B, to be

$$\Gamma = \frac{\mu}{2} \sqrt{\frac{(\mu + \rho)^2 + \pi^2\sigma^4}{\rho^2 + \pi^2\sigma^4}} \quad \text{and} \quad \phi = \arctan\left[-\frac{\rho^2 + \mu\rho + \pi^2\sigma^4}{\mu\pi\sigma^2}\right]. \tag{2.38}$$

Considering the limits of the plane wave and the point source, the argument of the Fresnel function needs to be real valued. From equation (2.37) it is easily seen that ϕ has to equal $-\frac{\pi}{2}$ in both the plane wave and the point source case. As it was stated that the diffraction pattern was visible if the (absolute) value of the argument of F [...] was smaller or equal to 10 and greater than -1 , equation (2.37) gives the range where diffraction fringes are visible. This range thus equals

$$-\sqrt{\frac{\mu}{2}} \left(\frac{(\mu + \rho)^2 + \pi^2\sigma^4}{\rho^2 + \pi^2\sigma^4} \right)^{\frac{1}{4}} \leq M \leq 10\sqrt{\frac{\mu}{2}} \left(\frac{(\mu + \rho)^2 + \pi^2\sigma^4}{\rho^2 + \pi^2\sigma^4} \right)^{\frac{1}{4}}. \tag{2.39}$$

Of course this, as well as ϕ , has to converge to the plane wave and point source range in limiting cases. For the plane wave case, with $\sigma = \infty$, this is immediately clear. For the point source case, $\sigma = 0$, and then equation (2.39) reduces to equation (2.19), obviously with x_s in equation (2.19) equal to 0 since it has been assumed the Gaussian beam is centered at the edge of the semi-infinite opaque screen.

As mentioned, the phase of the Fresnel function determines its shape. As already shown, the phase of the Fresnel function is 0 in case of the plane wave and the point source. In the region where the phase does not equal 0, deviations from the plane wave and point source diffraction pattern could be seen. The degree to which the shape deviates from the case where this phase equals 0 depends on the degree to which the imaginary part of the Fresnel function is present compared to the real part. Since the imaginary part will in general be approximately equal zero, it is more convenient to consider the quotient of real part to the imaginary part of $\exp[-\frac{i}{2}(\phi + \frac{\pi}{2})]$ instead of just the imaginary part of $\exp[-\frac{i}{2}(\phi + \pi)]$. As long as this equals -1 , the shape is like the one for the point source and the plane wave. However, as this fraction approaches zero (it cannot be more negative than -1) the shape of the diffraction form factor deviates strongly, as is shown in Figure 11. These Figures show that the interference fringes of the diffraction form factor become increasingly large by already slightly lowering the absolute value of the quotient. While the fringes get enhanced,

the spacing between the fringes does not change by adapting the quotient. This shows the number of fringes is determined by the absolute value of the argument in the Fresnel function and the shape is determined by its phase.

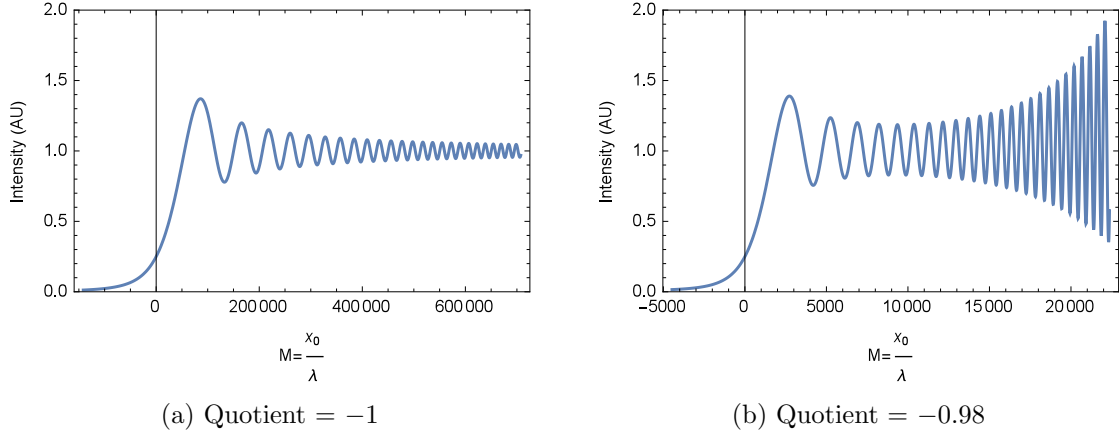


Figure 11: The form of the diffraction pattern for different values of the quotient of the real part to the imaginary part of $\exp[-\frac{i}{2}(\phi + \pi)]$

The logical question which follows is the physical interpretation of the increasing amplitude of the fringes. Increased amplitude of the fringes would imply more constructive (and destructive) interference. The quotient is only unequal to -1 in the range between the plane wave and the point source. Regarding the phase of a Gaussian beam when it moves from the region where it resembles a plane wave to the region where it resembles a point source, it is shown by equation (2.27b) that the phase front could only be planar, elliptical or circular. This would imply that an elliptical wavefront would increase the amplitude of the fringes. However, taking a look at equation (2.35), there is the Gaussian fall-off term in the expression of the intensity distribution. It could be that this term decreases faster than the fringes increase in amplitude and that as a result the total diffraction pattern does not show any stronger fringes than compared to plane wave diffraction and point source diffraction.

2.5.3 Intensity profile diffracted Gaussian beam - Gaussian fall-off term

In this section an elaboration on the Gaussian fall-off term in equation (2.35) has been done. As mentioned in the preceding, it is important to know how fast the Gaussian fall-off term decreases since it might compensate the increased fringe maximum. Therefore it would give insight if the width (rms) of the Gaussian fall-off could be determined. From equations (2.35) and 2.31 it is clear that the width of the Gaussian fall-off depends on w_0 , r_0 , and z . Next it seems convenient to express the width in dimensionless form, so equations (2.36) will be used.

As equation (2.35) indicates, the intensity pattern scales with $\left|\exp\left(\frac{\beta^2}{4\gamma}x_0^2\right)\right|^2$. Using the definitions of β in 2.32 and γ in (2.31) this can, as shown in appendix C, be rewritten to

$$\exp\left(\frac{2M^2}{\sigma_{rms}^2}\right), \quad \text{with} \quad \sigma_{rms}^2 = \sigma^2 + \frac{(\mu + \rho)^2}{\pi^2 \sigma^2}, \quad (2.40)$$

where σ_{rms} indicates the dimensionless, scaled to λ width of the Gauss. It could be shown that the beam size in the y -direction is equal to the beam size in the x -direction due to the

azimuthal symmetry of the Gaussian beam. Returning to the important aspect whether the Gaussian fall-off term decreases faster than the fringes increase in amplitude. Numerical simulations do show that the Gaussian fall-off term does decrease faster than the amplitude of the fringes increases.

Having acquired a dimensionless definition of the width of the Gaussian envelope, the entire diffraction pattern can be described dimensionless as follows

$$|\psi(x_0, y_0, r_0 + d_0)|^2 = \exp \left(\frac{2M^2}{\sigma_x^2 + \frac{(\mu+\rho)^2}{\pi^2 \sigma_x^2}} \right) \left| 1 + (1 - i)F \left[\sqrt{\frac{1}{\Gamma}} \exp \left(-\frac{i}{2} \left[\phi + \frac{\pi}{2} \right] \right) M \right] \right|^2, \quad (2.41)$$

with Γ and ϕ defined as in equation (2.38).

2.5.4 Off axis Gaussian beam and slit geometry

Up till now, the derivation has been done for a Gaussian beam that is centered on axis with the semi-infinite opaque screen. However, in reality it is certainly possible that the center of the Gaussian beam is off axis with the screen. Suppose the height of the center of the Gaussian beam above the screen is x_s , as indicated by Figure 10. To derive at the equations describing the diffraction of an off axis Gaussian beam, x in equation (2.29) is replaced by $x - x_s$. Since the screen is infinitely long in the y -direction, nothing changes to the y -direction of the description.

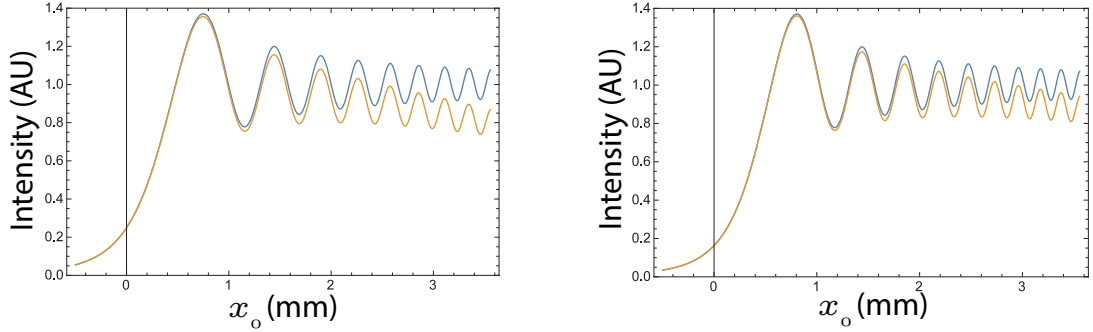
As a consequence of the replacement of x by $x - x_s$, it can be derived that additional terms arise in equation (2.35). In the Gaussian fall-off term x_0 will just be replaced by $x_0 - x_s$. Next to this an additional term in the argument of the Fresnel function will arise. This additional term equals $\frac{2}{\sqrt{\pi(1-i)}}x_s$. Expressing the argument of the Fresnel function again in terms of T and ϕ then gives

$$|\psi(x_0, y_0, r_0 + d_0, x_s)|^2 \propto \exp \left(\frac{2(M - S)^2}{\sigma_x^2 + \frac{(\mu+\rho)^2}{\pi^2 \sigma_x^2}} \right) \left| 1 + (1 - i)F \left[\sqrt{\frac{1}{\Gamma}} \exp \left(-\frac{i}{2} \left[\phi + \frac{\pi}{2} \right] \right) (M - S) + \frac{2}{\mu} \sqrt{\Gamma} \exp \left(\frac{i}{2} \left[\phi + \frac{\pi}{2} \right] \right) S \right] \right|^2, \quad (2.42)$$

where $S = \frac{x_s}{\lambda}$, the dimensionless height. This shows that due to x_s the Gaussian fall-off is only shifted, which is as expected since the center of the Gaussian beam would not change by diffraction on a semi-infinite opaque screen.

This expression reduces to the absolute value squared of equation (2.7) when the waist of the beam, or rather the Rayleigh length, becomes large compared to d_0 and r_0 . This is seen by taking the limit of $\sigma \rightarrow \infty$ in T , which then equals $\sqrt{\frac{\mu}{2}}$. This is in accordance with what is expected, since a Gaussian beam with an infinite waist actually a plane wave. In Figure 12a the diffraction pattern for a plane wave is shown together with the diffraction pattern of a Gaussian beam. In these plots, all parameters that appear in the plane wave case as well as in the Gaussian beam case are set to the same value. In the Gaussian beam case, w_0 is so large that the Rayleigh length is 500 times r_0 . Although the position of the fringes in the

Gaussian beam pattern is the same as for the plane wave, the Gaussian fall-off is still visible. The decrease in fringe amplitude in the region shown becomes smaller as the Rayleigh length further increases.



(a) Fresnel diffraction pattern of a plane wave (blue) and a Gaussian beam with $z_R = 500r_0$ (orange)
(b) Fresnel diffraction pattern of a point source (blue) and a Gaussian beam with $z_R = 500r_0$ and $z_R = 500d_0$ (orange)

Figure 12: The form of the diffraction pattern for different values of the quotient of the real part to the imaginary part of $\exp\left[-\frac{i}{2}(\phi + \pi)\right]$

On the other hand, when the Rayleigh length of the beam becomes small compared to r_0 and d_0 , equation (2.42) reduces to the absolute value squared of equation 2.16. Again this is in accordance with what is expected, since a Gaussian beam with an infinitely small waist actually is a point source. This resemblance is shown in Figure 12b, where the Fresnel diffraction pattern of a perfect point source is shown together with the Fresnel diffraction pattern of the Gaussian beam. Again, all the parameters that appear in both geometries are set to the same value. The Rayleigh length in the Gaussian beam diffraction is 500 times smaller than d_0 and r_0 .

Depending on the degree to which a Gaussian beam resembles a point source x_s is of importance and as was shown in the point source diffraction x_s shifts the diffraction pattern downwards if its value is positive and upwards if it is negative. This also holds for the diffraction form factor of the Gaussian beam. However, x_s also influences the center of the Gaussian fall-off term and here the effect is the opposite. If x_s is positive, the Gaussian fall-off term shifts upwards. Since the diffraction pattern of a Gaussian beam is the product between the fall-off term and the diffraction form factor, changing x_s changes the intensity of fringes relative to each other. This has been made visible in Figure 13, where the intensity of the fourth fringes still is nearly equal to the intensity of the first fringe which is obviously not the case in Figure 12. Figure 13 also shows how the regular diffraction pattern of a Gaussian beam actually looks. In this Figure the Gaussian Fall-off term has been plotted in orange to show that the diffraction fringes do indeed follow the Gaussian envelope.

Table 2: Parameters of diffraction pattern in Figure 13

Relevant parameter	Value
w_0 (μm)	74.9
r_0 (mm)	200
d_0 (mm)	800
x_s (mm)	0.85
λ (nm)	632.8
z_R (mm)	28

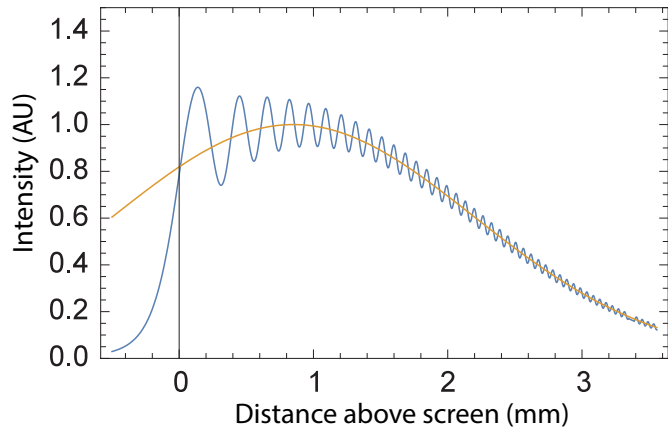


Figure 13: Diffraction pattern (bleu) of a Gaussian beam and the Gaussian envelope (orange)

Next to the diffraction pattern in Figure 13 the Gaussian fall-off term is also shown. It is clear that the diffraction does indeed follow the Gaussian envelope as expected.

Having proven relation (2.42), one could by the same method arrive at the equation describing the diffraction of a Gaussian beam on a slit with width D_{slit} . To arrive here, the upper integration border is not infinity but equals D_{slit} . The effect of this is that $(1 - i)$ in equation (2.42) is replaced by $\sqrt{2}$ and the term 1 before the Fresnel function is replaced by another Fresnel function. This Fresnel function has an equal argument to the other Fresnel function, only with S replaced by $S - \Delta_{slit}$, and the entire argument then has to be multiplied by -1. Here Δ_{slit} is the dimensionless slit width defined as $\frac{D_{slit}}{\lambda}$.

3 Experimental setup

3.1 Experimental setup for testing theory on gaussian beam diffraction

The theory of Fresnel diffraction of a plane wave and a point source on a semi-infinite opaque screen have been derived in section 2. These two wave forms are limiting cases of the Gaussian beam. This theory could be tested using the setups shown in Figure 14 and Figure 15 below. In these setups a JDS Uniphase 1103P HeNe-laser with a wavelength of 632.8 nm is used as light source, or rather a source of waves. This laser emits a Gaussian beam with a TEM00 mode purity over 95% [14]. Lenses in the setup are used to expand or contract the beam to give the waist of the Gaussian beam the desired physical dimension. To measure the diffraction patterns a CCD camera is used, which is a “Point Grey Fly cam FL2-08S2M” model type. This CCD camera has a pixel size of $4.65 \mu\text{m}$ and 1032×776 pixels [15] and is situated in the plane indicated by D in Figure 14.

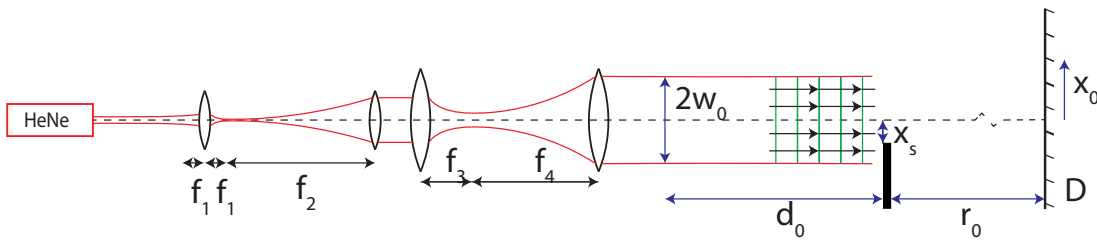


Figure 14: Setup used to detect Fresnel diffraction of a plane wave. Two lens systems are used to expand the beam in order for the Rayleigh length to be much larger than d_0 and r_0 , which are the distances between the beam waist and the semi-infinite opaque screen and between the semi-infinite opaque screen and the CCD detector respectively. The misalignment of the semi-infinite opaque screen with the center of the beam waist is defined as x_s .

The diffraction object whereon diffraction takes place is an aluminum plate. This aluminum plate is the bottom side of a $200 \mu\text{m}$ slit used in a monochromator. This slit is cut in the middle, so it has become a sharp edge. As shown in Figure 14 the height of the center of the beam above the edge of the semi-infinite opaque screen is indicated by x_s . To investigate the effect of x_s , this value has to be changed in experiments. This could be done by changing the position of the HeNe, and the two telescope systems. However it is practically more convenient to change the height of the semi-infinite opaque screen instead of the center of the beam. So to investigate the influence of x_s on the diffraction pattern, the height of the semi-infinite opaque screen is adapted instead of the height of the beam that comes falls on the semi-infinite opaque screen.

The setup shown in figure 14 is used to detect the Fresnel diffraction pattern of a plane wave. A “real” plane wave obviously has a infinite beam waist, but the essence of a kind of diffraction is the form of the wave front in the plane were diffraction takes place.

As mentioned in section 2.4.2 the Rayleigh length has to be larger than d_0 and r_0 than z_R in order to simulate a plane wave Gaussian beam. Here where d_0 and r_0 are the distance between the beam waist and the slit and the distance between the slit and the CCD camera as shown in figure 14. The size of the beam waist is indicated by w_0 and the coordinate along the CCD camera is x_0 . This CCD camera is used to observe the diffraction pattern. In the setup of the plane wave two lens systems are used to expand the beam originating from the

HeNe laser 40 times. This has been done by first expanding the beam with a telescope system that has two lenses with focal lengths of 15 mm and 150 mm. After this expansion the beam is expanded by the second telescope system that has lenses with focal lengths of 25 mm and 100 mm. The top of the semi-infinite opaque screen could be, on purpose, misaligned with the center of the Gaussian beam (the dashed line in Figure 14). The degree of misalignment is x_s and is also shown in Figure 15. The beam waist of the HeNe laser is specified to be 630 μm . Using an expansion of 40 and formula for the Rayleigh length in equation (2.30) the Rayleigh length is larger than 3.1 km. In the setup d_0 and r_0 are between 10 cm and 1 m, wherefore the wave does resemble a plane wave at the semi-infinite opaque screen.

The beam size behind the telescope system has been measured. Three measurements of the beam size have been done, see appendix D. No divergence is measured between 50 cm and 212 cm behind the lens, but there is a divergence between 212 cm and 482 cm. The angle of divergence in this range equals 3 milliradian. The maximum divergence of a Gaussian beam having a beam waist of 1 cm can be derived by dividing the beam size, equation (2.27a), by z when z is much larger than the Rayleigh length. Here this divergence equals $\frac{\lambda}{\pi w_0} = 2 \cdot 10^{-5}$ radian. This is 2 orders smaller than the 3 milliradians just mentioned which indicates the lenses of the telescope system possibly disturb the wave front of the incoming beam and that therefore the beam could not be described as a first order Gaussian beam.

The opposite of a plane wave is the point source which has a beam waist that is infinitely small and has a spherical wavefront. To reach at a situation where the wave front is spherical at the plane of diffraction, d_0 must exceed z_R substantially. This could be done by making d_0 very large or by minimizing z_R . For practical convenience the Rayleigh length is minimized using the setup shown in figure 15. Here a microscope lens is used to minimize the beam waist.

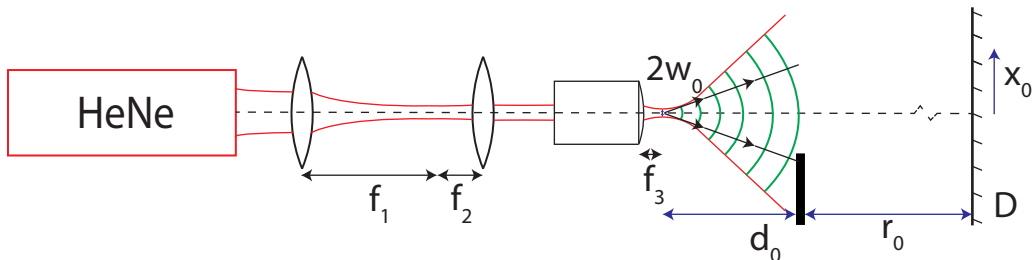


Figure 15: Setup used to detect Fresnel diffraction of a point source. A microscope lens is used to blow up the beam in order for the Rayleigh length to be smaller than d_0 , which is the distance between the beam waist and the semi-infinite opaque screen. The misalignment of the center of the beam and the semi-infinite opaque screen is x_s and the distance between the semi-infinite opaque screen and the CCD detector is r_0 .

Using this setup the beam waist is contracted 4 times by the lens system (focal lengths of 25 mm and 100 mm) and eventually focused by a microscope lens. This microscope lens has a magnification factor of 63 and a numerical aperture of 0.75. Therefore the beam is approximately contracted to the diffraction limit of this microscope lens. Using that the aperture of the microscope lens is completely used and that the numerical aperture is 0.75, the diffraction limit of the microscope lens is approximately 0.42 μm . This means the Rayleigh length is smaller than 1 μm which implicates that the beam has a circular wave front if the screen and the camera are positioned in the centimeter range behind the microscope lens.

The telescope system is used for the following: without the telescope system, the beam would have a size considerably larger than the aperture of the microscope lens. Therefore the beam will be cut by the lens, which creates diffraction from the lens itself. This diffraction acts as noise, since it alters the wavefront falling on the screen's edge. To diminish this effect a telescope system has been used to decrease the beam size so it will show less diffraction from the microscope lens.

In between the plane wave and the point source approximations of the Gaussian beam, there is a regime where the wavefront of the Gaussian beam is not planar nor it is spherical. This regime is called the “intermediate case”. To observe Fresnel diffraction of a Gaussian beam with a wavefront as in the intermediate case, d_0 needs to be in the order of the Rayleigh length, z_R . Since the width of the Gaussian beam equals $630\text{ }\mu\text{m}$, the Rayleigh length equals 2.0 m . So the Rayleigh length is in the same order of length as d_0 and r_0 . Therefore no lenses are used. The setup used to observe the Fresnel diffraction of the intermediate case is shown in Figure 16.

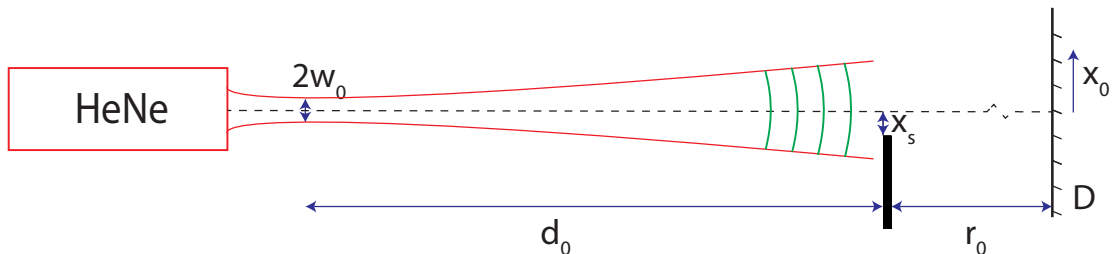


Figure 16: Setup used to detect Fresnel diffraction of the intermediate case. The beam only expands by its own diffraction and the distance between the beam waist and the semi-infinite opaque screen, d_0 , is in the order of the Rayleigh length. The misalignment of the center of the beam and the semi-infinite opaque screen is x_s and the distance between the semi-infinite opaque screen and the CCD detector is r_0 .

With the three setups shown in this section, all the relevant ranges of the Gaussian beam could be investigated. In this setup adaptions could be made in the distances d_0 and r_0 to investigate their influence on the diffraction pattern and compare it with the theory developed in section 2.

3.1.1 Beam waist calibration and CCD resolution verification

In the previous text it has been stated that lenses or a microscope lens are used to blow up or minimize the beam waist so to create the desired wavefront of the Gaussian beam. In case of plane wave diffraction or point source diffraction, the Rayleigh length is made either a couple of order larger than r_0 and d_0 or a couple of orders smaller by the lens systems. Therefore the exact value of the beam waist is not important in these cases. In the intermediate case however there were no lens systems present and the beam with the beam waist generated from the HeNe laser diffracts on the semi-infinite opaque screen. Therefore the value of the beam waist is important in case of the intermediate case diffraction.

As derived in section 2.4 equation 2.27a, the waist of the beam evaluates as

$$w(z) = w_0 \sqrt{1 + \left(\frac{z\lambda}{\pi w_0^2} \right)^2}, \quad (3.1)$$

which will be used to calibrate the beam waist. To determine the beam waist, and its position, from (3.1), the waist of the Gaussian beam is measured at different distances from the HeNe laser. Thereafter this relation, with z replaced by $z - z_0$, is fitted through the data. The addition of z_0 is to compensate for the fact that the measurement starts at the output of the HeNe laser, whereas $z = 0$ in equation (3.1) is defined as the position of the beam waist. Using this fit, z_0 is the distance of the HeNe laser output to the beam waist. The waists at different positions from the HeNe output are shown in Figure 17.

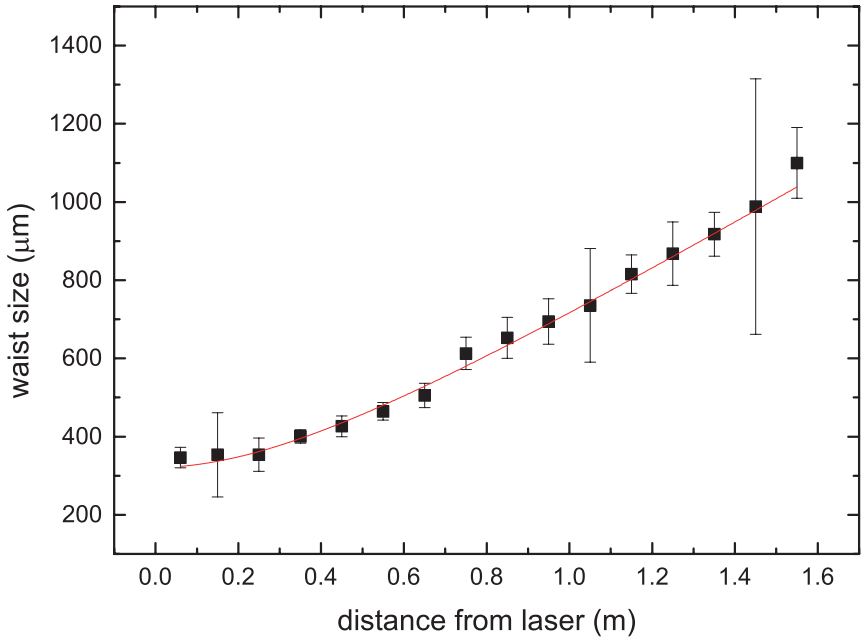


Figure 17: Waist of the beam as function of the distance from the laser. Equation (3.1) has been fitted through the data with z replaced by $z - z_0$ in order to determine the waist position and the beam waist size

From the fit w_0 is determined to be $(320 \pm 5)\mu\text{m}$, which is equivalent to a Rayleigh length of 0.51 m , and z_0 is determined to be $(2 \pm 1) \cdot 10^{-2}\text{m}$. This means that the beam waist is twice as small as stated in the specifications [15]. Therefore the Rayleigh length of the setups above is 4 times smaller. This does however not change the facts that the Gaussian beam resembles for example a plane wave in the first setup.

Next to the calibration of the beam waist, the resolution, or pixelsize, of the CCD camera is verified. This has been done by placing a slit with a width of 1 mm as close to the camera as possible. Normally the CCD camera has a glass plate in front of it, which causes Fizeau fringes on the CCD camera for monochromatic laser beams. These Fizeau fringes serve as noise to the measurement. To reduce this noise, the glass plate has been removed. By removing the glass plate, the CCD chip is exposed to air and dust. By coupling an OD filter to the CCD camera, the CCD chip is not exposed to the air and dust. This OD filter however sets a boundary for the minimal distance between the slit and the place where the CCD chip of the CCD camera is located. This minimal distance is approximately 37 mm. For best verification of the pixel size the setup of the plane wave case is used. The reason behind this choice is the following. Suppose a point source case was used, then the diffraction pattern would spread out further in the geometric shadow than it would in the plane wave case. This is due to the fact that the beam comes from one point and therefore it makes an

angle with one of the slits which basically results in a shifting of the diffraction pattern. So to make the diffraction pattern as minimal in the geometric shadow, a plane wave setup is used.

First a simulation has been done on what the diffraction pattern of the slit would look like. This diffraction pattern is shown on the left side of Figure 18. The red lines in this Figure indicate where the edges of the slit are situated, so one at zero and one at 1 mm.

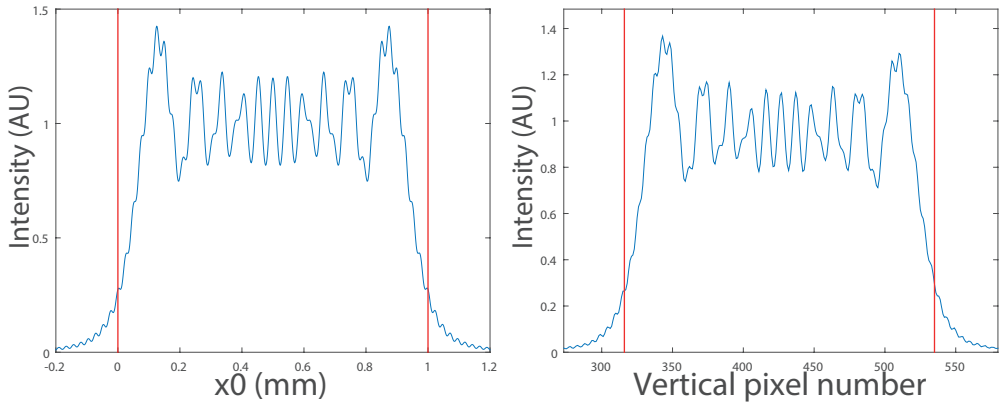


Figure 18: Left is the analytical pattern of a 1000 micron slit placed 3.7 cm in front of the CCD camera. The red lines indicate where the slit actually is. Right is the experimental data shown.

The data acquired from the experiment is shown on the right side of Figure 18. Now the horizontal axis contains pixel numbers and the red lines indicate again the positions of the slits edges. The positions of these red lines in the experimental diffraction pattern are determined in the following way. In the analytical pattern the value of the intercept between the red line and the diffraction pattern at $x_0 = 0$ can be found. Since the slit is symmetric the same value is the intercept at $x_0 = 1\text{mm}$. This value then is divided by the maximum intensity of the diffraction pattern, so the value of this interception point is normalized by the maximum intensity of the diffraction pattern. To find the position of the slits edges in the experimental data the reversal process has been done. First the maximum of the intensity distribution is found. Subsequently this value is multiplied with the normalized interception point of the analytical pattern, lets call the resulting value the reference value. The position of the slits edges then are the points where the intensity of the experimental data equals the reference value.

The resolution is determined by dividing the width of the slit, 1 mm, by the number of pixels between the red lines shown in the right Figure of Figure 18. Since a pixel number is an integer and the position where the experimental data equals the reference value, the pixel numbers where the slits edges are are the rounded values. This is taken into account by using an uncertainty of one pixel .The result of this verification is a resolution of $(4.56 \pm 0.01)\mu\text{m}$ per pixel in both the horizontal and the vertical direction. This agrees within 2% compared with the specifications of the CCD camera [15]. Since the method used is not infinitely accurate but agrees within 2% with the specifications, it has been assumed in the following that these specifications are true.

4 Results and Discussion

The diffraction theory stated in section 2 covers the entire range from point source diffraction through the intermediate case diffraction to the plane wave diffraction. This theory is tested using the setups shown in section 3.1 for the three different cases. In this section results on these tests will be discussed. First the plane wave diffraction will be considered followed by the point source diffraction. At last, the intermediate case will be discussed. Before discussing the results from the experiments a elaboration on the correction of noise on the data acquired is given.

4.1 Plane wave diffraction

As stated in section 3.1 the Rayleigh length in the plane wave setup (Figure 14) exceeds d_0 and r_0 , which allows one to describe the diffraction pattern by the theory developed in section 2.2 for plane wave diffraction. In the setup of Figure 14 different lengths of r_0 could be chosen in order to test the influence of r_0 on the diffraction pattern.

4.1.1 Plane wave noise correction

Before the analysis of the diffraction pattern of the plane wave a procedure is used to correct the measured diffraction image from noise. In order to do this, first a “background image” has been measured. In the background image the semi-infinite opaque screen has been taken out of the setup. The measured background image is shown in Figure 19a. After the background image is measured, the Fresnel diffraction pattern is measured. In Figure 19b the measured diffraction pattern is shown before the noise correction.

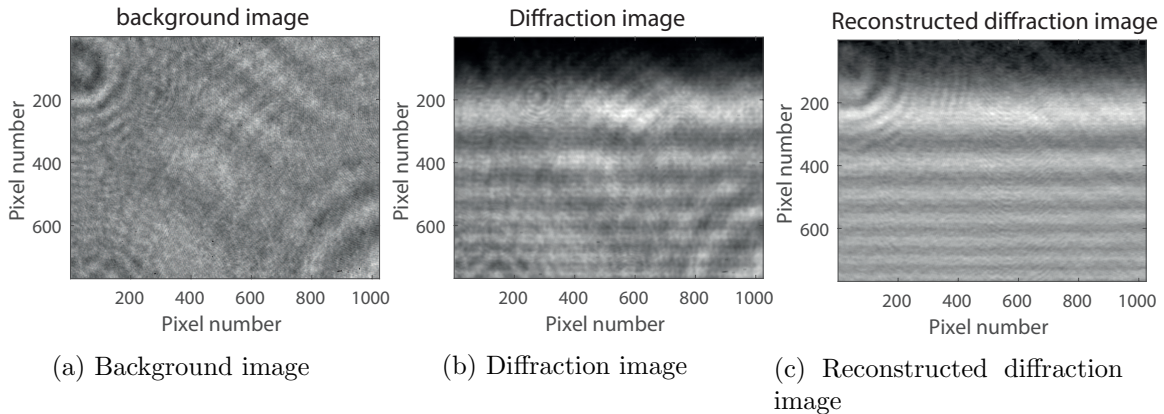


Figure 19: The background image is shown in the left Figure and is used together with the middle image to make the right image.

Since the waist of the beam in this setup is large compared to the size of the CCD camera ($40 \cdot 320 \mu\text{m} = 12.8 \text{ mm}$ compared to 4.8 mm) the intensity of the background image can in theory be approximated by a constant. This is used to reduce the noise in the diffraction image of Figure 19b. From the diffraction image the background image, which includes the same noise as the diffraction image, is subtracted. This action reduces the noise in the diffraction image, but also creates “negative intensities” at places where the diffraction intensity is lower than the intensity of the background image. To compensate for this, the

average of the background image is added to the noise reduced diffraction image. The result is of this procedure is shown by comparing the region below the highest fringe in Figure 19b and Figure 19c.

The advantage of this method is that the noise in the region of diffraction is compensated. The disadvantage is that this method creates noise in the geometric shadow region. This noise actually is the negative of the noise in the background image. This noise is added since the background image, which has light in the region above the place where the first fringe would occur (geometrical shadow region), is subtracted from the diffraction image, which has no light in the geometrical shadow region. Eventually then the average of the background image is added again to create a “negative” of the noise in the background image. But since the diffraction mainly occurs in the geometrical light region, the noise in the geometrical shadow region is not a severe issue. In theory, a better method to compensate for the noise is to divide the diffraction image by the background image. However due to noise there are some zero intensity points in the background image. Since division by 0 is not allowed, the above mentioned method is used. This method turns out to be appropriate in this experiment.

As is visible from Figure 19a the noise in the background image exists of some circles and to a lesser extend the noise also consist of some diagonal fringes. The origin from these diagonal fringes is the OD filter. These fringes actually are Fizeau fringes from the OD-filters. The circles arise from dust on the OD filters in front of the camera and dust on the lenses in the setup. It has been tried to remove this dust, but this did not seem to work good enough to vanish these circles. However, as is seen by comparing the reconstructed diffraction image with the diffraction image, these circles and Fizeau fringes could partially be removed numerically, which makes cleaning the lenses and the OD filters less necessary. The reconstructed diffraction image namely does not show these circles and shows a clear diffraction fringe pattern.

Since the fringe pattern is, in theory as well as based on Figure 19, symmetric it would be enough to consider just one vertical line in the reconstructed image. To further reduce noise however, the mean value of every row is used as data that will be considered to analyze the diffraction pattern.

4.1.2 Analyzing Fresnel diffraction patterns of a plane wave

Through the data acquired by the noise correction method the absolute value squared of equation (2.7) multiplied by I_0 and with x_0 replaced by $x_0 - x_v$ is fitted. This means the fit function is

$$I = I_0 \frac{1}{4} \left| 1 + (1 - i) F \left[\sqrt{\frac{2}{r_0 \lambda}} (x_0 - x_v) \right] \right|^2. \quad (4.1)$$

Including I_0 takes care of the intensity of the diffraction pattern. Replacing x_0 by $x_0 - x_v$ compensates the fact that the $x_0 = 0$ zero-point on the CCD camera is not on axis with the edge of the semi-infinite opaque screen. This is only a shifting and has no further physical implications.

The diffraction images shown in Figure 19 have been measured in a situation where r_0 is 80 cm. The data acquired from this diffraction pattern by the taking the mean of every row is shown in Figure 20. The fit function of equation (4.1) is fitted through the data. Since the wavelength of light from a HeNe laser is 632.8 nm, this value has been used for λ in the fit function. The values of the fit parameters and their uncertainties are shown in Table 3

and are determined by the least square method.

Table 3: Fit parameters and expected values

Parameter	value	68% (\pm)
I_0	0.973	0.001
x_v (mm)	0.363	0.001
r_0 (m)	1.215	0.001

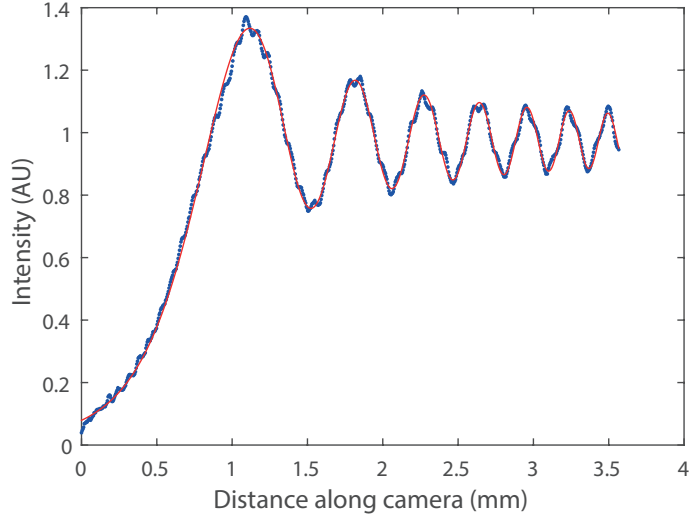


Figure 20: Experimental data (blue) fitted with equation (4.1)

As is visible in Figure 20 the fit function perfectly describes the experimental data. Additionally the fit parameters have uncertainties which are smaller than 1% as compared to the value of the fit parameter itself. However, there is a very important result to notice from Table 3, namely that in the fit in Figure 20 the value of r_0 equals 1.215 m, whereas in the setup r_0 was set to 80 cm. In the following three aspects are discussed that could possible explain this deviation.

- In section 3.1 it has been discussed that the telescope system possibly disturbs the wave front and therefore the beam can not be described any more as a first order Gaussian beam. This might be a reason for the deviation of the value of r_0 .

It could be that the beam is cut by the fourth lens in the setup of Figure 14 and that therefore the beam is not Gaussian anymore, but a diffracted beam. In this setup, the diameter of the lens that possibly cuts the Gaussian beam equals 3.8 cm. Whether Fresnel or Fraunhofer diffraction occurs is determined by the Fresnel number stated in section 2. In this setup the Fresnel number, with r_0 is equal to an exaggerated value of 1.5 meter, equals 39. This means the diffraction still is far in the Fresnel limit. Fresnel diffraction of a plane wave extends to a region of $10\sqrt{\frac{r_0\lambda}{2}}$, see equation (2.11). So with the values in this setup, the Fresnel diffraction at 1.5 meter extends 7 mm from the edge. The center of the beam therefore is not influenced at 1.5 meter from the lens, and could therefore be described by the same way as before the lens. So since the measured diffraction is approximately 4 mm in the center of the diffracted beam, the cutting of the Gaussian beam also not account for the deviation of r_0 .

- One other possibility is that the CCD chip is not perpendicular to the propagation direction of the beam and is positioned under an angle. These CCD chips are however manufactured so that when the body of the camera is perpendicular to the propagation of the beam, the CCD chip is also perpendicular to the beam propagation. It has been tried to position the CCD under 15 degrees from the propagation direction. This is a large angle and it is seen by eye that the CCD chip is not tilted by 15 degrees compared to the body of the camera. Putting the body of the camera under 15 degrees (and therefore the CCD chip is

also turned by 15 degrees) made a difference of 10 cm in the value of r_0 , see appendix E. However, 10 cm still does not account for the difference in the fit value from 80 cm. So the angle position of the CCD is not the cause of this difference.

- What has been noticed during the experiment is that the position of the last lens is important for the fit value of r_0 from different fits through different data. Therefore it has been investigated what the relation is between the lens position and the fit value of r_0 . Of course, changing the lens position is actually changing the size of the beam waist and the position of the beam waist. So actually it would be desirable that a relation between the size of the beam waist, the beam waist position and r_0 could be investigated. However, due to reasons concerning time and concerning space in the lab, this has not been done extensively. In the following a relation between the lens position, measured compared to some reference position, and the fit value of r_0 is presented. This relation is given in Figure 21.

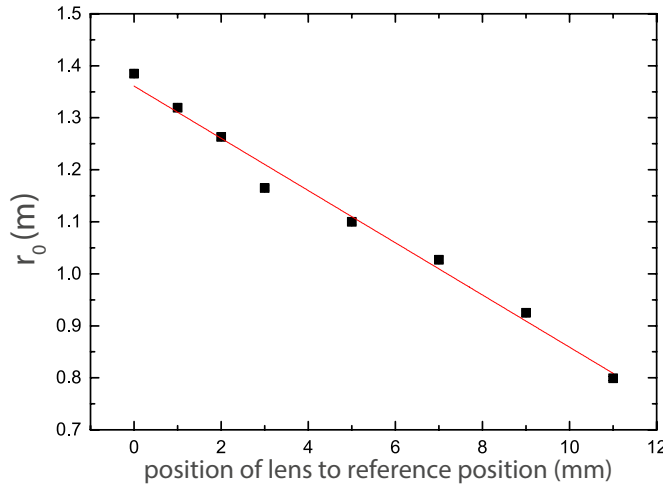


Figure 21: The relation between r_0 from the fit of the absolute value squared of equation (2.7) and the position of the lens compared to a reference position. Through the data a linear function is fitted.

There seems to be a linear relation between the fit value of r_0 and the position of the last lens. Therefore a linear relation is fitted through the data points in Figure 21. This resulted in an offset, of (1.36 ± 0.02) m and a slope of (5.0 ± 0.2) cm/mm. Figure 21 indicates that there is a point where the r_0 from the fit will be 0.8 m, which would imply that that particular position is the right position of the lens to simulate a plane wave. However, it is seen by eye that the beam is convergent in the region where the CCD camera is positioned and that therefore the beam does not resemble a plane wave.

So in short, the lens position of the last lens is very influential on the value of r_0 that one gets from the fit with equation (4.1). There is one position of this lens for which r_0 is actually the expected value, 80 cm. But with the lens in this position, it is even evident by eye that the beam is convergent, which would not be so in the plane wave case. It is thus probable that the last lens, or the entire second telescope system introduces severe imperfections to the beam. To investigate whether this is true and to analyze a different resemblance of a plane wave, the last telescope system is removed for new measurements

4.2 Plane wave diffraction with a smaller waist

By removing the last telescope system, the beam is magnified by a factor 10 instead of 40. This means the beam waist of the Gaussian beam in this situation equals (3.2 ± 0.5) mm.

With this beam waist three different setups regarding d_0 and r_0 have been tried and will be discussed below. Bear in mind that d_0 is not the distance between the lens and the semi-infinite opaque screen, but it is the distance between the beam waist and this screen. It is however strongly related to d_0 . Important to know is that in these setups, the intensity is by approximation not constant over the CCD chip. With the second telescope system in place, this approximation was valid. The validity of this approximation could easily be checked by calculating the ratio of the width of the Gaussian beam over the diffraction range, so the fraction of the σ_{rms} in expression (2.40) over the right hand side of expression (2.39). If this fraction is much larger than one, the approximation of constant amplitude over the CCD chip is valid. If this value is in the same order as 1, this approximation is not valid. The three setups and their specifications, including the value of the fraction just mentioned, are shown in Table 4 below:

Table 4: Specifications of the three setups in the plane wave diffraction

	r_0 (cm)	Distance lens-screen (cm)	$\frac{\sigma_{rms}}{\text{Diffraction range}}$
Setup 1	80	20	0.64
Setup 2	50	50	0.80
Setup 3	20	80	1.27

None of the fraction values in Table 4 is much larger than one, so the constant amplitude approximation is not valid anymore in these setups. Therefore, a new method of enhancement of the diffracted image has been used. Previously the background image was subtracted from the diffraction image to eventually add the mean of the background image again. The method for image enhancement, or noise correction, in this setup is discussed below.

4.2.1 Noise correction in plane wave smaller waist setup

First a background image is measured. In this background image the maximum value and the position of the maximum value is found. Next to the maximum value, also the e^{-2} intensity points and their positions have been found. From these positions the beam width could be determined. Using the value of the beam waist, the maximum value and its position, a theoretically ideal Gaussian beam is reconstructed. The measured background image is shown in Figure 22a and the reconstructed background image is shown in Figure 22b.

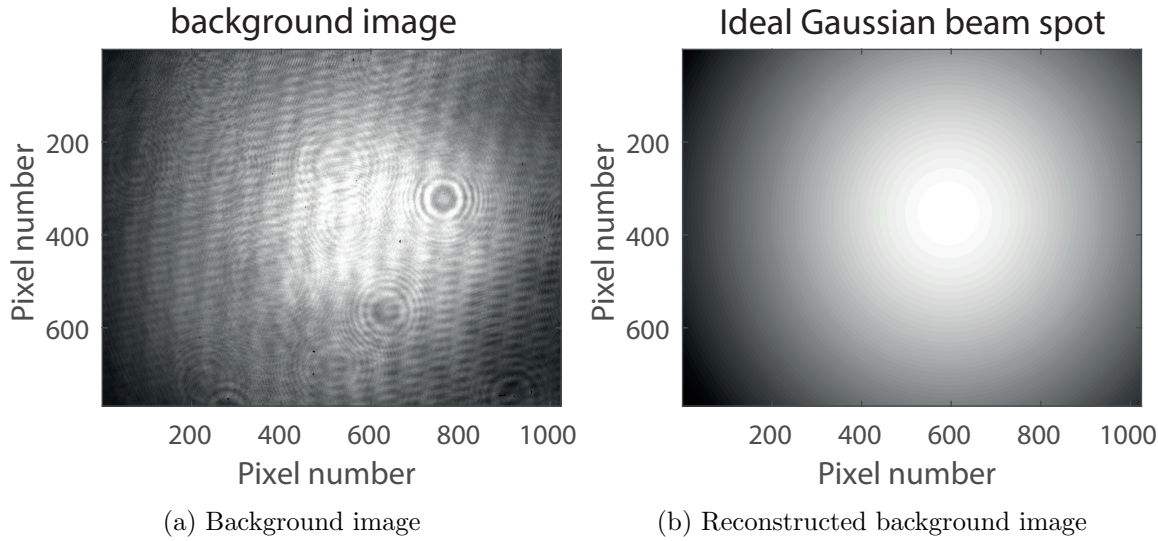


Figure 22: The background image and the reconstructed background image of the plane wave smaller waist setup

Second, the diffraction image is measured. From this image the background image is subtracted and the reconstructed background image, an ideal Gaussian beam, is added. As was in the plane wave case with the initial setup, this creates noise in the region where no light has been observed. Again, since in this region, no real information is stored, the addition of noise is not a real drawback in this method. Now the image has been fully reconstructed. However, one additional operation is desirable. In the plane wave of the previous setup, the intensity of the pixels in the horizontal direction could be averaged without concern since the pattern was symmetric and the intensity was constant. Now the pattern again is symmetric, but the intensity is not constant. So averaging over the horizontal direction would in this case imply that pixels near the center of the Gaussian beam weigh more than away from the center. Of course, their intensity is larger, but this does not mean any other form of a diffraction pattern is measured. The intensity of diffraction effects are linear with the intensity. So to make an equal weighting the reconstructed image is divided by a Gaussian in the horizontal direction. The measured diffraction image is shown in Figure 23a and the diffraction image after the mentioned procedure is shown in Figure 23b. The data to analyze the Fresnel diffraction pattern then is the average over the horizontal direction.

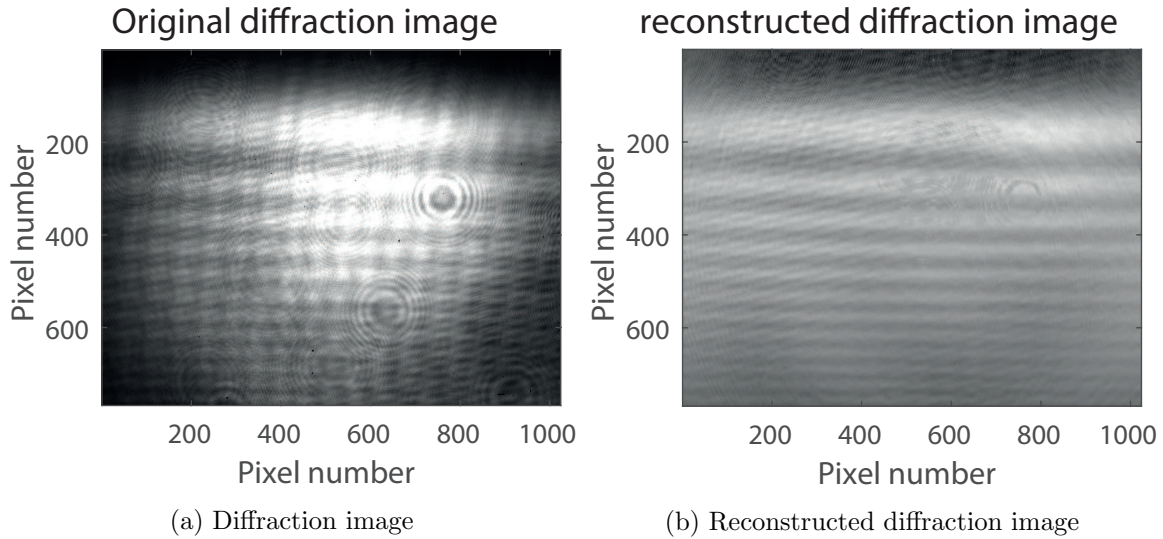


Figure 23: The diffraction image and the reconstructed diffraction image of the plane wave smaller waist setup

The goal of the enhancement of the images is to analyze the data from the diffraction image. In the following the three setups mentioned above will be discussed, starting with the setup with r_0 equal to 80 cm.

4.2.2 Analyzing Fresnel diffraction patterns of a plane wave with a smaller waist

In each setup the diffraction pattern of three different situations has been measured. The only difference between these situations is the height of the screen. Figure 24 shows three datasets together with a fitted function. This data is acquired by the method explained above and the fit function used is equation (C.7) multiplied by I_0 to take account for slightly wrong normalization. Equation (C.7) is the dimension full intensity distribution of a Gaussian beam, so the dimension full form of (2.42). The diffraction patterns are normalized so that if there was no screen the maximum intensity equals one. In the fit function x_0 replaced by $x_0 - x_v$ to compensate for the camera-screen alignment and an offset is added since the diffraction image enhancement procedure allows the pattern to have non zero intensity minimum.

Through the data equation (C.7) will be fitted with the value of d_0 is set to 0 cm. This is allowed since a look at equation (C.7) shows that d_0 only appears in terms where it has to compete with the Rayleigh length, $\frac{\pi w_0^2}{\lambda}$. In this setup the beam waist equals approximately 3.2 mm and therefore the Rayleigh length equals 50 m. The beam does not diverge in the region behind the lens, which indicates that the beam waist is located near the semi-infinite opaque screen. Suppose the beam waist is 3 meter away from the semi-infinite opaque screen. Then d_0 would be 3 m, which still is approximately 17 times smaller than the Rayleigh length. Therefore the value of d_0 does not influence the diffraction pattern and could be set to 0. The values of I_0 and the offset are determined by setting them as a fit parameter in a first fit. Then in the second fit, these values are set before the fitting to the value of the first fit, leaving only x_v , x_s , w_0 and r_0 as fit parameters. The values of these fit parameters are shown in Table 5.

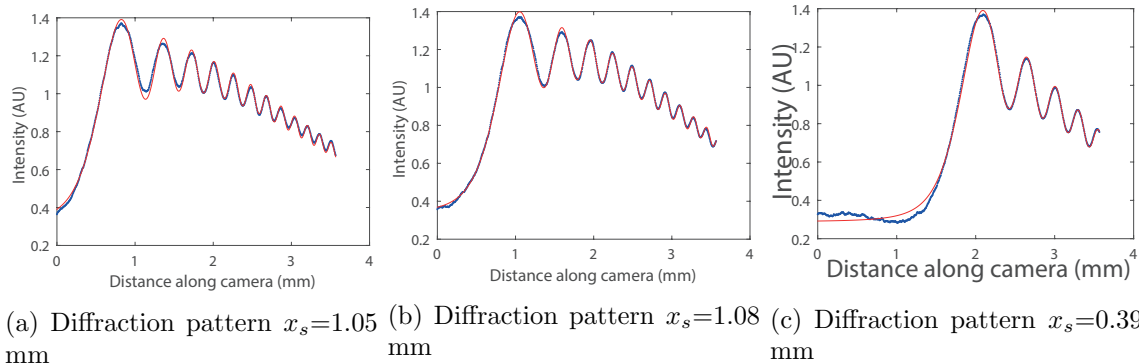


Figure 24: Three diffraction images where the only difference is the height of the point source compared to the semi-infinite opaque screen, x_s .

Table 5: Fit parameters of figures in 24

	x_v (mm)	x_s (mm)	w_0 (mm)	r_0 (cm)
Figure 24a	0.222	1.05	3.66	75.12
68% \pm Figure 24a	0.001	0.01	0.01	0.03
Figure 24b	0.444	1.084	3.25	76.00
68% \pm Figure 24b	0.001	0.004	0.01	0.06
Figure 24c	1.498	0.38	2.87	76.23
68% \pm Figure 24c	0.002	0.02	0.04	0.01

By comparing the diffraction patterns and the values of x_s it could be seen that the diffraction patters of 24b and 24c are shifted to the right compared to Figure 24a. However in Figure 24b the value of x_s from the fit is larger than in Figure 24a while in Figure 24c x_s is smaller. This is strange since in both Figures the pattern is shifted to the right. This can however be explained by the fact that the Rayleigh length is 50 m while r_0 is in the order of sub-meters and d_0 is set to 0. Using this it can be seen from equation (C.7) that the only influence x_s has on the diffraction pattern is a shifting of the Gaussian fall-off term. Since x_v also has this effect, an error in x_s could be compensated for in x_v .

Next thing to notice is that w_0 is different in all the three fits while nothing has chanced in the beam width. While the fit values of x_s could be explained by the fact that errors in x_s could be compensated by x_v there is no parameter that could compensate an error in w_0 . Namely the width of the Gaussian fall off is in this setup only determined by the beam waist. Actually the exact value of the beam waist does not seem to be very important in this case. This is indicated in Figure 25, where two theoretical patterns are compared. These patterns have both have the same parameters as the fit values of Figure 24a, except for the beam waist. In the blue line, the beam waist equals 3.66 mm and in the orange line it is 2.87 mm. What could be seen is that in the first 4 fringes these patterns do not differ considerably. So in this region the exact value of the beam waist is not very important. In the third fit for example only 5 fringes need to fitted, and since the two different patterns in Figure 25 do not differ considerably in the first 5 fringes the exact value of the waist is not very important here. So therefore deviations can occur in the fit value of w_0 . It has however to be noticed that the average of the three w_0 from the fits equals (3.26 ± 0.02) mm which is just 1.9% larger than the expected value of the beam waist.

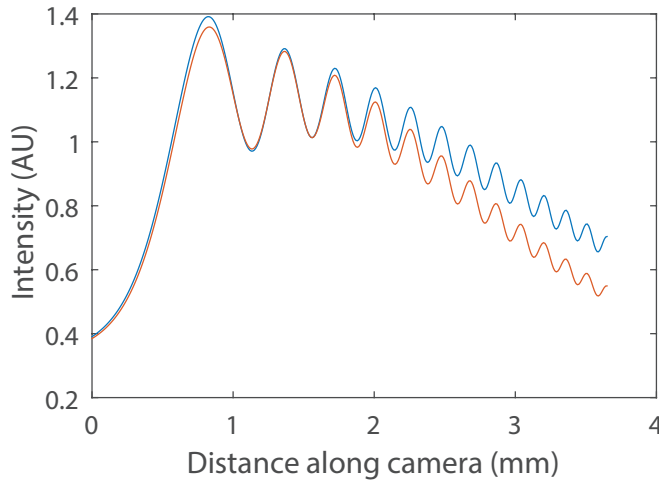


Figure 25: Two theoretical Fresnel diffraction patterns which only differ in value the beam waist. In the blue line $w_0 = 3.66$ mm and in the orange line $w_0 = 2.87$ mm

Finally it has to be noticed that the values of r_0 in the three different fits are all in between 75.1 cm and 76.2 cm. However, in the setup r_0 is determined to be 80 cm. This 80 cm however is a bit doubtful since it is not perfectly known where the CCD chip that actually measured the diffraction pattern is located. This could however only explain a difference of 1 cm in r_0 , while the deviation in the fits is 4 to 5 cm. It could possibly be that now the lenses of the first telescope system influence the beam in the same way as the second telescope in the plane wave diffraction with two telescope systems in place. To investigate whether this is true, in a next research the effect of the lens position of one of the telescope lenses on the fit value of r_0 could be investigated. The size of the beam behind these lenses did however not seem to change as was seen by eye, which is however inaccurate off course.

The second setup mentioned was the setup where r_0 equals 50 cm, so the semi-infinite opaque screen is 50 cm in front of the camera. In the same way as before measurements have been done and the same fit function as above has been fitted through this data. This has been visualized in figure 26 where again the only difference in the setup is the height of the screens edge compared to the middle of the Gaussian beam.

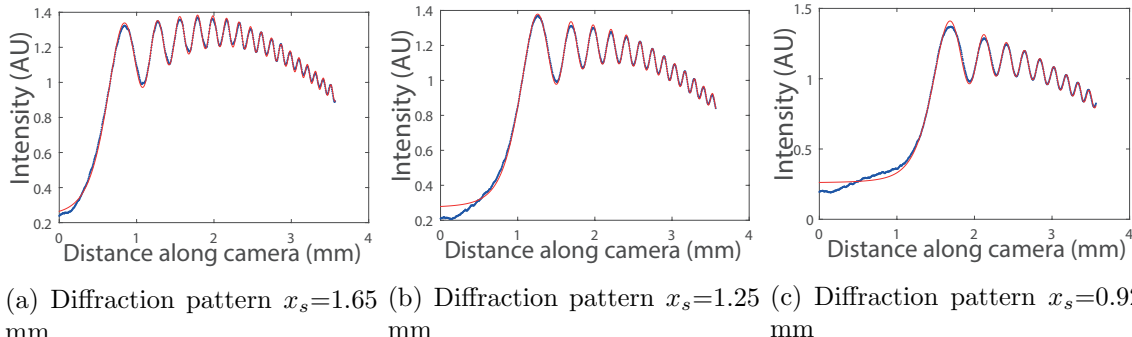


Figure 26: Three diffraction images where the only difference is the height of the point source compared to the semi-infinite opaque screen, x_s .

The fit parameters of the fits in Figure 26 are shown in Table 10 in appendix F. In this case

the values of x_s are consistent in the sense that in Figure 26c x_s is smaller than in Figure 26b and Figure 26a and that x_s in Figure 26b is smaller than in Figure 26a. However in the patterns where x_s is smaller, x_v is larger and therefore these values could compensate each other as has been told in the case where r_0 was 80 cm. What is however to be noticed is that the Gaussian fall-off in Figure 26a is visible, not the first fringe is at a maximum, but the fourth fringe is. In Figure 26c however, the first fringe is at a maximum again and actually only the right side of the Gaussian is visible. This would imply that by varying x_s the diffraction pattern actually shifts more than the Gaussian envelope. But as mentioned in the experimental setup, the effect of x_s is actually investigated by changing the height of the semi-infinite opaque screen. Relatively this is the same, so for the diffraction pattern it does not matter. It does however matter for the way the diffraction pattern is interpreted. By changing the screen's height instead of the height of the beam, the interpretation of the effect of x_s has to be turned around. So by varying x_s the Gaussian envelope shifts more than the diffraction pattern. This is also what is expected since the influence of x_s in this beam setup is only in the Gaussian fall-off term and not in the diffraction pattern as already mentioned in the setup where r_0 equaled 80 cm.

Table 10 in appendix F shows that the fit value of r_0 deviates from 50 cm. This could again be possibly explained by the lenses in the telescope system. Next to that the variation in the fit parameter w_0 could again be understood by 25.

Then there is the third setup with r_0 equal to 20cm. The diffraction patterns from this setup do not reveal any unknown facts about the influence of x_s on the diffraction pattern. However, as was derived in section 2.2 and is indicated by equation (2.10) the spacing of fringes is proportional to $\sqrt{r_0}$. This means that the fringe spacing in the third setup is smaller than in the first two. In Figure 27 diffraction patterns of all the three setups are shown and it can be seen that the fringe spacing indeed is larger when r_0 is larger.

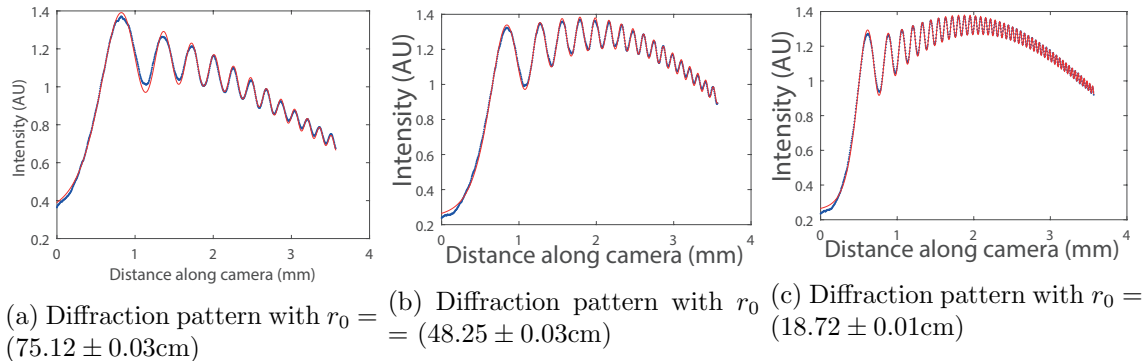


Figure 27: Three diffraction images where the only difference is the height of the point source compared to the semi-infinite opaque screen, x_s .

Equation (2.10) also shows the spacing dependence on the number of the fringe and tells that the spacing between fringes decreases as the fringe number increases. This is also verified by Figure 27.

So far for three different plane wave setups have been discussed. This has shown four main conclusions. One is that the fit function used (nearly) perfectly fits the acquired data. second, the exact value of the beam waist is not very important. Third it has been seen that there could really be made a separation between a diffraction pattern and the Gaussian

envelope and that the position of this Gaussian envelope with respect to the diffraction pattern is determined by x_s . The last conclusion is that the fringe spacing becomes smaller as r_0 becomes smaller as was expected based on (2.10)

4.3 Point source diffraction

Along the plane wave resemblance of the Gaussian beam, where the screen and the camera are placed far inside the Rayleigh range, the Gaussian beam could also resemble a point source. For the Gaussian beam to resemble a point source, the screen and the camera must be far outside the Rayleigh length. By placing d_0 and r_0 in the orders of centimeters, this is already verified as mentioned in the experimental setup (section 3.1). In the point source diffraction, noise correction has also been done. Again, first the method of noise correction is discussed where after Fresnel diffraction patterns are analyzed.

4.3.1 Point source noise correction

As has been mentioned in the plane wave case the diffraction images that come directly from the camera contain a lot of noise. This is even worse in the point source case since the effect of dust particles is magnified due to the large focusing of the microscope lens that finally results in a magnification of the dust/noise. Therefore an image enhancement procedure is also necessary in the point source case. The image enhancement procedure in the point source case is the following: First a background image has been measured. Then the diffraction image is measured. From this diffraction image the background image is subtracted and thereafter the mean value of the background image is added again to compensate for negative intensities. Adding the mean value of the background image is allowed since the $\frac{1}{e^2}$ beam size at the plane of the camera, which is 50cm behind the microscope lens in this setup, is 25 times the size of the CCD chip. This has the effect of deleting the noise in the region where the diffraction fringes are visible. However, it creates a “negative” of the noise in the geometric shadow region behind the screen in the same way as in the plane wave case. Figure 28 shows this procedure for the point source diffraction.

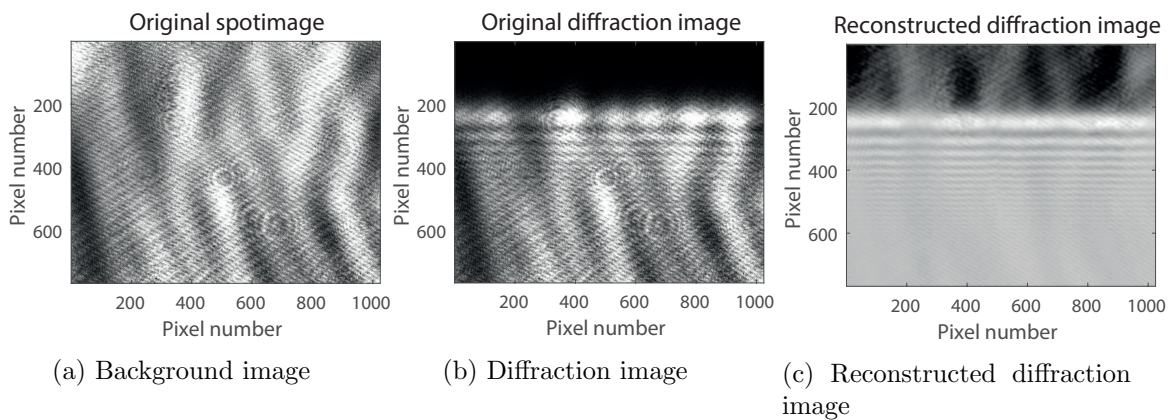


Figure 28: The background image is shown in the left Figure and is used together with the middle image to make the right image.

To achieve at data that is analyzed there is averaged over the pixels in the horizontal direction of Figure 28c. This does further decrease the noise in the fringe region, but does not reduce

the noise in the geometrical shadow region desirably. However, since no physical information is stored in the geometrical shadow region this is of little importance. In fitting the theory of point source diffraction data points in the geometrical shadow region are not included in the fit.

4.3.2 Analyzing Fresnel diffraction patterns of a point source

In the plane wave case three different setups have been investigated where r_0 was set to three different values. In the point source case also three different setups have been investigated. Here however the distance between the beam waist and the semi-infinite opaque screen, d_0 is important, whereas it was not important in the plane wave case since it was small compared with the Rayleigh length. In the three setups the values of d_0 and r_0 have been changed, but their sum always was 50cm. These values are shown Table 6. Notice that here d_0 is equivalent to the distance between the microscope lens and the semi-infinite opaque screen since the position of the focus of the microscope lens is (by approximated) directly behind the lens.

Table 6: Specifications of the three setups in the point source diffraction diffraction

	r_0 (cm)	d_0 (cm)
Setup 1	35	15
Setup 2	25	25
Setup 3	15	35

The fit function used in the point source case is the intensity distribution of the point source diffraction derived in section 2.3. This is the absolute value squared of equation (2.16). As has been seen in the plane wave case x_0 had to be replaced by $x_0 - x_v$ to take into account that the screen and CCD camera are not perfectly aligned and since x_s is changed by shifting the height of the screen while not changing the height of the CCD camera. However, as has been shown in section 2.3 changing x_s only shifts the diffraction pattern by a factor $\frac{r_0}{d_0}x_s$. So actually x_s and x_v have the same effect: they both shift the diffraction pattern. Therefore they are interchangeable for the fit function and the fit function could make no distinction between them. For this reason, in the fit function the parameter x_s is used to fit the entire shifting of the diffraction pattern. Again, for reasons concerning normalization procedures of the intensity a factor I_0 is added. Also an offset is added since the diffraction pattern does not start at zero intensity. This means that the resulting fit function equals

$$I = \text{OffSet} + I_0 \frac{1}{4} \left[\left| 1 + (1 - i) F \left(\sqrt{\frac{2}{\lambda}} \left(\frac{1}{d_0} + \frac{1}{r_0} \right) \frac{d_0 x_0 + r_0 x_s}{d_0 + r_0} \right) \right|^2 \right]. \quad (4.2)$$

As mentioned, the effect of x_s is the same as the effect of x_v . Therefore effects of x_s and x_v are the same. This actually means that it is not possible to verify the shifting behavior of x_s since this could also be accounted in x_v . For this reason, just one setup (one value of x_s) has been tested in the three setups. The diffraction pattern measured in the setup with r_0 equal to 35 cm is shown in Figure 29.

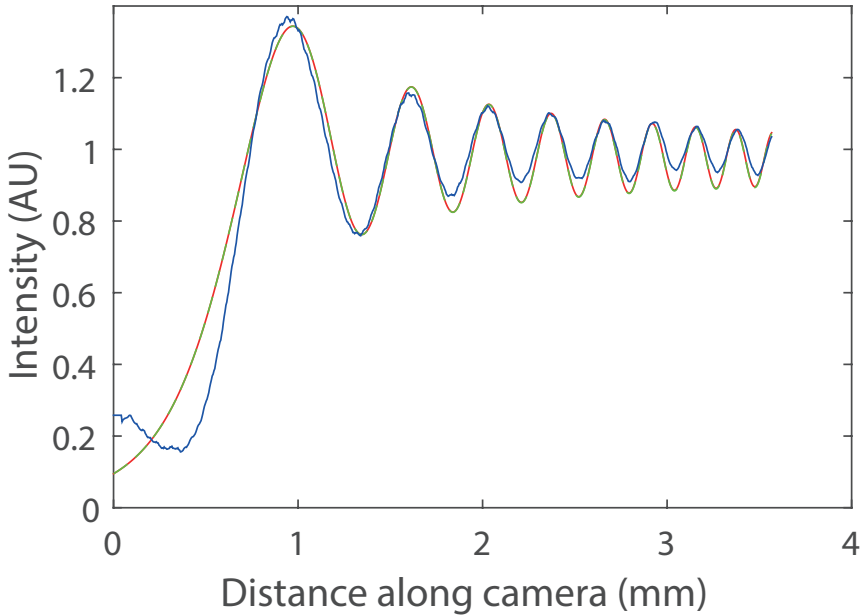


Figure 29: Diffraction pattern of the point source (blue) with fits through it with a preset value of d_0 (green) and with a preset value of r_0 (red)

Through this data equation (4.2) is fitted in two different methods. In the first method only I_0 , OffSet, x_s and r_0 have been set as fit parameters and d_0 and λ have been set manually. Of course λ is set to 632.8 nm, d_0 is set to 15 cm since this distance is also by approximation equal to 15 cm in the experimental setup. This fit is shown in the green. In the second fit, r_0 is set manually and d_0 is set as fit parameter. The value of r_0 is set to 35 cm since this is by approximation the value for r_0 as in the experimental setup. This fit is shown by the red line. Since I_0 and OffSet do not influence the form of the diffraction pattern the only relevant parameters actually are x_s , d_0 and r_0 , where x_s only shifts the diffraction pattern. The relevant fit parameters are shown in Table 7.

Table 7: Fit parameters of figures in 29

Fitvalues	x_s (mm)	d_0 (cm)	r_0 (cm)
Fit with d_0 manually $68\% \pm 29$	-0.129	15	32.43
	0.001	0	0.04
Fit with r_0 manually $68\% \pm 29$	-0.144	18.13	35
	0.002	0.04	0

What has to be noticed is that the red and green fit in Figure 29 perfectly follow each other. They also follow the data except for the intensity minima. However, the values of d_0 and r_0 in these two fits are obviously different. What this tells is that not only x_s and x_v are interchangeable for the fit function, but also d_0 and r_0 . Therefore it is necessary to set one of these values manually. As can be seen the fit value of r_0 is deviates from the value in the experimental setup, 35cm. Also the fit value of d_0 deviates from the value in the experiment, 15cm. Since they are interchangeable, the origin of this deviation must be the same. One possible explanation could be that the telescope system or the microscope lens influences the wave front of the beam. To test whether this actually is the origin, the same experiment

could be done using different lenses.

The second setup in the point source diffraction is the setup with both d_0 and r_0 equal to 25 cm. In the third setup d_0 equals 35 cm whereas r_0 equaled 15 cm. In the plane wave case the fringe spacing was smaller when r_0 became smaller and became larger when r_0 became larger. In Figure 30a the diffraction patterns (blue) and the fits (red and green) of the second point source setup is shown. In Figure 30b the diffraction pattern (blue) with the fits (red and green) of the third setup are shown.

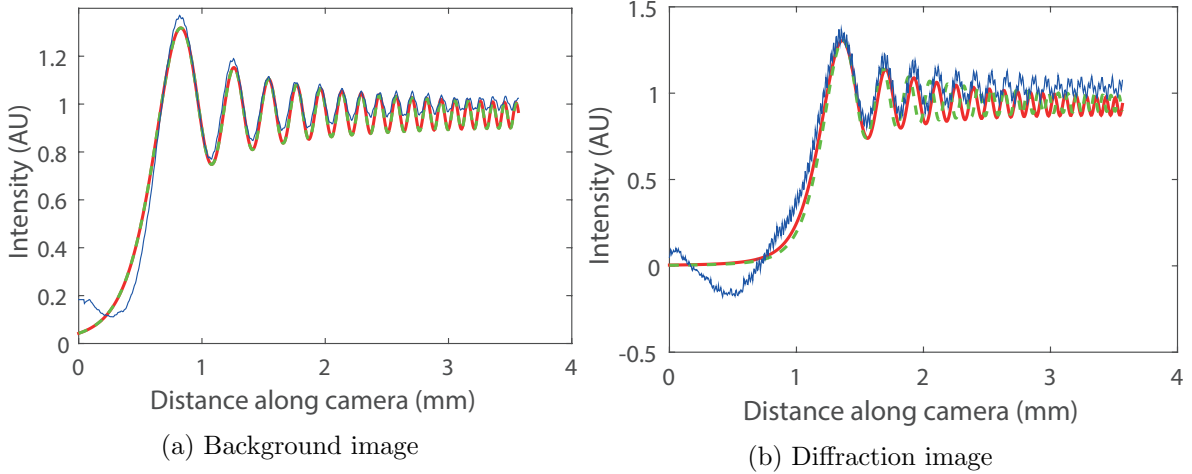


Figure 30: The background image is shown in the left Figure and is used together with the middle image to make the right image.

The values of the fit parameters are shown in Table 8.

Table 8: Fit parameters of figures in 29

Fit values	x_s (mm)	d_0 (cm)	r_0 (cm)
Fit in Figure 30a with d_0 manually $68\% \pm 30a$	-0.383 0.002	25 0	23.69 0.02
Fit in Figure 30a with r_0 manually $68\% \pm 30a$	-0.430 0.003	29.6 0.1	25 0
Fit in Figure 30b with d_0 manually $68\% \pm 30b$	-2.17 0.01	35 0	16.59 0.04
Fit in Figure 30b with r_0 manually $68\% \pm 30b$	-1.08 0.01	16.3 0.1	15 0

Table 8 shows that if d_0 is set manually to the value it approximately is in the experimental setup, r_0 agrees within 1.7 cm with its value in the setup. However, if r_0 is set manually to the value of the setup, then d_0 differs 4.6 cm from the 25 cm as it was in the setup of Figure 30a. The fit value of d_0 in the third setup is off by 18.7 cm from the value it is in the setup, 35 cm. What this tells is that when d_0 is set manually the result of the fit parameter r_0 better approaches its experimental value. Regarding at the interchangeability of d_0 and r_0 , Table 8 tells that to compensate r_0 by d_0 , d_0 deviates more from its experimental value than r_0 when d_0 is compensated by r_0 .

For the story just mentioned one has to take into account that the green, and to a lesser

extent the red, fit do not follow the data in Figure 30b. In Figure 30a the fits do follow the data in the sense that the fringes of the fit and the data are located at the same positions (in the minima of the fringes the fit intensity of the fit is lower).

As mentioned in the plane wave case, the fringe spacing increases when r_0 is increased. From equation (2.18) it is seen that also d_0 influences the fringe spacing. This equation actually comprises all the information of the fringe spacing. To experimentally test the influence of d_0 on the fringe spacing, experiments have to be done when r_0 is fixed. This has not been done here. But since the fit of the point source diffraction converges on the data, relation (2.18) has actually implicitly been verified by the experiments above and therefore the dependence of the fringe spacing on d_0 .

4.4 Intermediate case diffraction

In the plane wave case and the point source case some beautiful Fresnel diffraction pictures clearly showing the fringe pattern have been measured. In the plane wave case the screen and the camera were placed “far” inside the Rayleigh range whereas in the point source diffraction the screen and the camera have been placed “far” outside the Rayleigh range. The remaining question is: is the theory developed in section 2.5 confirmed by experiments? In this section an answer is given by measured diffraction patterns and comparisons with what would be expected.

In this section the diffraction pattern of one setup with d_0 equal to 80cm and r_0 equal to 20cm will be shown where x_s is varied to see its influence. Next the diffraction pattern of three different setups is analyzed to see the influence on the fringe spacing of d_0 and r_0 . First, a noise correction method will be discussed.

4.4.1 Intermediate case noise correction

Also in the intermediate case setup a noise correction procedure has been applied to diffraction image measured. In this setup however, no lenses were used. Therefore no noise is generated by dust or aberrations on/of lenses. The only parts in the setup that could cause any noise are the OD-filters in front of the CCD-camera. Since the beam size is small compared to the dimension of the OD-filter, the beam could propagate through a part of the OD-filter where little dust, and therefore little noise, is. Next to dust on OD-filters, the OD-filters also create Fizeau fringes on the CCD-camera. These two noise effects of the OD-filters are small and no extensive noise correction procedure has been applied. However, to reduce the (closely) spaced Fizeau fringes, every pixel is averaged over a rectangle of pixels around it, where the width of this rectangle was 25 pixels and the length 5 pixels. The width is larger than the length which is logical since the diffraction effects of the screen are symmetric in the horizontal direction, the direction wherein the width is defined. If one would average over a large number of fringes in the vertical direction, the length direction, then next to averaging out Fizeau fringes, diffraction effects would also be averaged out. The data to analyze eventually is acquired by extracting the column containing the maximum of the measured diffraction image.

The diffraction pattern measured on the CCD-camera is shown in Figure 31a, the data before the averaging is shown in Figure 31b and the data after the averaging is shown in Figure 31c.

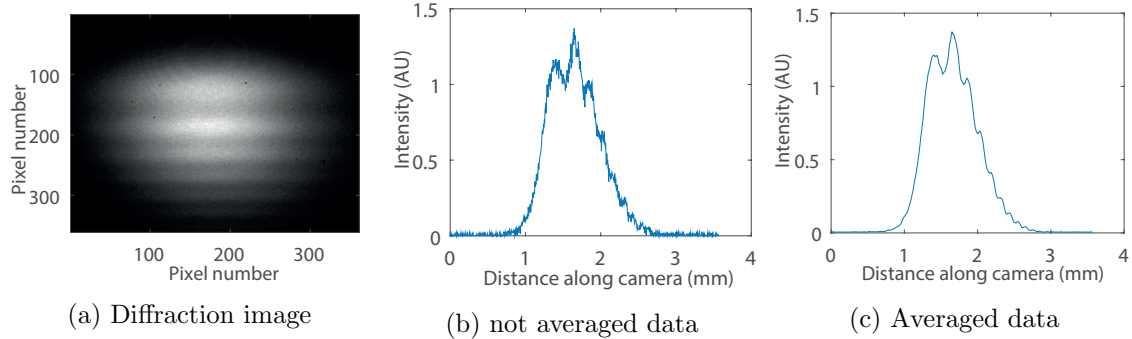


Figure 31: The background image is shown in the left Figure and is used together with the middle image to make the right image.

The data shown in Figure 31c shows no further image enhancement procedure is needed since noise is barely seen on this data

4.4.2 Analyzing Fresnel diffraction patterns of an intermediate case Gaussian beam

In Figure 32 three diffraction patterns of an intermediate case Gaussian beam are shown. Through the data from these diffraction patterns fit function (C.7) is fitted, again multiplied with I_0 and x_0 replaced by $x_0 - x_v$. These diffraction patterns have been measured in a setup with d_0 equal to 80 cm and r_0 equal to 20 cm. The only difference between the three figures is the height of the center of the Gaussian beam compared to the screen's edge.

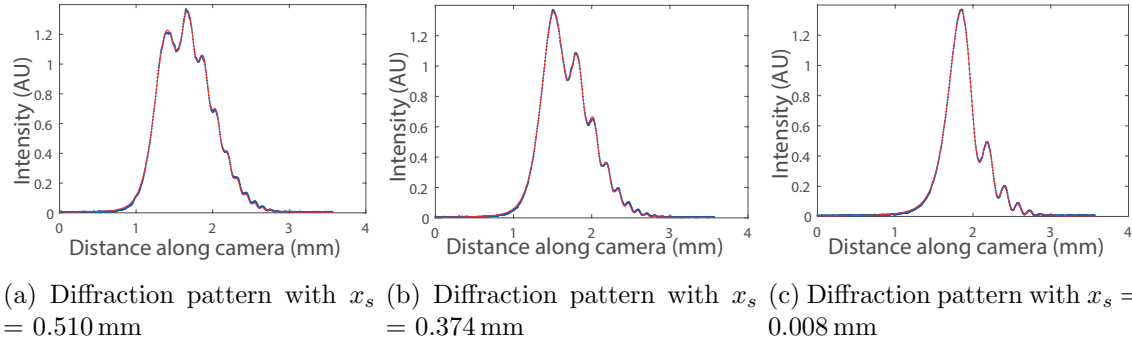


Figure 32: The background image is shown in the left Figure and is used together with the middle image to make the right image.

The values of the fit parameters are shown in Table 9. From the Figures above it can be seen that the fit function describes the pattern nearly perfectly. However, the values of r_0 and d_0 do deviate from their values in the experimental setup. Especially d_0 deviates considerably and on top of that it is different in the three fits. Since the Rayleigh length in this setup is 50 cm, d_0 certainly is important and has to be taken into account. Simulations do however show that varying d_0 in the range from 80cm to 95cm does not considerably shift the diffraction pattern, but only changes the amplitude of the fringes. Since the amplitude of the fringes is of less importance than the form of the pattern, these deviations of d_0 from 80cm are acceptable.

Table 9: Fit parameters of figures in 32

Fit value	x_s (mm)	d_0 (cm)	r_0 (cm)
Figure 32a	0.510	83.7	21.41
68% \pm Figure 32a	0.001	0.1	0.04
Figure 32b	0.374	85.4	21.65
68% \pm Figure in Figure 32b	0.001	0.1	0.02
Figure 32c	0.008	95.5	21.63
68% \pm Figure in Figure 32c	0.001	0.2	0.02

An important aspect that Figure 32 shows is the multiplication between the diffraction form factor and the Gaussian fall-off, and their dependence on the height of the Gaussian beam compared to the screen's edge.

In the diffraction pattern of Figure 32a, not the first fringe is the maximum fringe, but the second one. This means the Gaussian envelope has shifted to the right in this figure compared to the diffraction pattern. In Figure 32b, x_s is smaller than in Figure 32a. Based on the theory developed on the Gaussian beam diffraction this would imply that the diffraction form is shifted upwards and the Gaussian fall-off term is shifted downwards and that therefore the maximum of the pattern shifts to the first fringe. This is indeed noticed in Figures 32b and 32c. In Figure 32c x_s is even lower than in Figure 32b which means the diffraction form is shifted upwards even more and the Gaussian fall-off is shifted downwards. This actually says that the diffraction form factor is located more on the tail of the Gaussian fall-off term and therefore less fringes are visible. Indeed, this is verified by comparing Figure 32c to Figure 32b.

As was observed in the plane wave case, where the Rayleigh length is larger than d_0 and r_0 , increasing r_0 leads to a larger spacing of the fringes. When the Rayleigh length is smaller, so in the point source case, d_0 is also on influence on the fringe spacing. In between the plane wave and the point source there is the Gaussian beam and therefore it is expected that d_0 and r_0 are also both of influence in the spacing of diffraction fringes in the Gaussian beam diffraction.

In Figure 33 the Gaussian beam diffraction is shown for three different setups. In these setups d_0 and r_0 have been changed compared to each other.

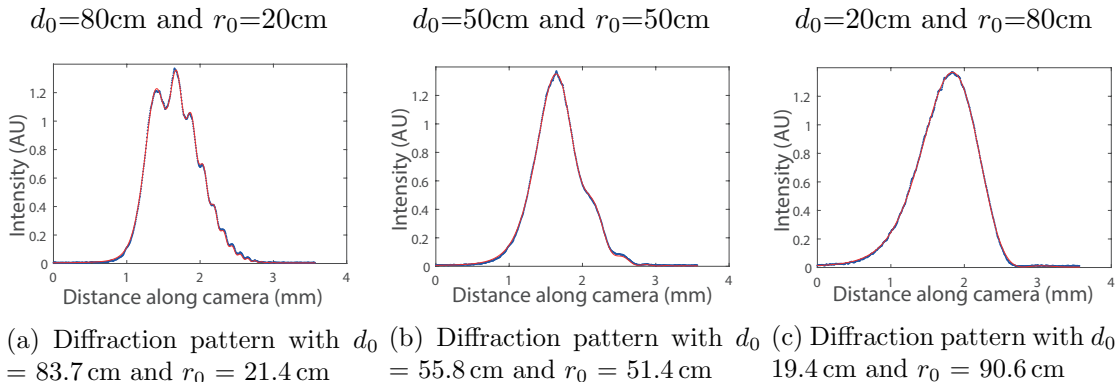


Figure 33: The background image is shown in the left Figure and is used together with the middle image to make the right image.

What is seen by comparing the three figures in Figure 33 is that in Figure 33a fringes are

visible and spaced closely and that in Figure 33b some “bumps” are visible while in Figure 33c no fringe or bump is visible anymore. This could be understood by the dependency of the fringe spacing on r_0 and d_0 and the dependence of the width of the Gaussian fall-off term on these parameters. It can be derived that the width of this fall-off term does depend on r_0 and d_0 , however, it only depends on the sum of these parameters (see equation (C.7) appendix C). It also depends on the dimension of the beam waist, but this value is fixed in the setup. Additionally, the values of r_0 and d_0 in the experiment are set in such a way that their sum is always the same. Therefore the width of the Gaussian fall-off in all the three figures of Figure 33 is the same.

Next to this fall-off term, the diffraction pattern of a Gaussian beam also consisted of a diffraction form factor. In this diffraction form factor fringes are visible and the spacing between these fringes does depend on r_0 and d_0 . It increases if r_0 is increased and if d_0 is decreased. Going from Figure 33a to Figure 33c the value of r_0 increases and the value of d_0 decreases. This means that theoretically the fringe spacing would increase. This is actually observed. In Figure 33a the fringes are clearly visible, however in Figure 33b some “bumps” are visible. These bumps actually are diffraction fringes, but their intensity is decreased by the Gaussian fall-off term. And the larger the fringe spacing is, the further a fringe is on the tail of the Gaussian fall-off, the more its intensity is decreased by the Gaussian fall-off term. So a larger fringe spacing also means that fringes are less good visible.

This is beautifully illustrated by Figure 33c where the fringe spacing is even larger than in Figure 33b. Here, the fringe spacing between the first and second fringe is approximately equal to or even greater than the width of the Gaussian fall off term. Therefore the second fringe gets already killed by the Gaussian fall-off term and as a result no fringes are visible. Thus increasing the fringe spacing decreases the visibility of the fringes since the fall-off term kills the fringes that are near the tail of the fall-off.

5 Fresnel diffraction and coherence of electron beam

In the UCP setup of the CQT lab electron beams are used for example to do diffraction experiments on samples. For these experiments to show useful information, the coherence length of the electron beam needs to be larger than the typical length of the sample. Based on this restriction and the fact that electron beams are partially coherent, one first needs to know whether the coherence length of the electron beam used is large enough. In his thesis, W.J. Engelen measured the emittance of a beam using a waist scan[16]. In a waist scan the beam size is measured as a function of the position as the beam passes through its waist and from this the emittance can be determined. The emittance of a beam is related to the brightness of a beam that could be used to determine the quality of an electron beam[17][1]. The focusability of a beam increases with increasing degree of coherence and therefore the minimal beam size decreases when a beam becomes more coherent. At a certain degree of coherence, the focusability becomes so strong that the size of the beam is smaller than the resolution of the camera detecting the beam waist. Therefore the actual size of the beam waist can not be measured and a new method of determining the degree of coherence has to be used.

A method to determine the quality is based on Fresnel diffraction. In section 2 a theory of Fresnel diffraction has been developed. Herein the Fresnel diffraction pattern of a Gaussian beam has been derived that was unknown in literature. In section 4 the theory was shown to be consistent with experiments.

Before discussing on how Fresnel diffraction could be used, the definition of C_x called the

degree of coherence is given. Here, C_x is defined as

$$C_x = \frac{L_x}{\sigma_x} \quad (5.1)$$

where L_x is the coherence length of the electron beam and σ_x is the rms beam size of the electron beam. The parameter C_x actually tells how much of the total size of the beam is coherent. This is a rough description of coherence. If one would describe coherence very accurately one should take into account first order and higher order coherence functions [18]. Since the goal of this section is to serve as a basis for determination of the degree of coherence of an electron beam, the above description of degree of coherence is allowed.

In his article, N. de Jonge used Fresnel diffraction of an electron beam on a circular hole in a TEM grid to determine the Brightness of its electron beam[1]. He calculated the Fresnel diffraction pattern of one point source and thereafter convoluted this pattern with a Gauss that had a width equal to the source size of the electron beam. The electron beam N. de Jonge used could be thought of being build up from point sources. Then taking the convolution just mentioned is basically taking the incoherent weighted sum of the diffraction patterns of all the point sources where from the beam is build up. The effect is that the fringes of the Fresnel diffraction pattern decrease in visibility. The degree to how many fringes are still visible/countable is a measure for coherence [1]. How to imagine these point sources in the Gauss is illustrated by Figure 34 where the total beam (green) is build up of point sources, the red dots. The degree to which a diffraction pattern of a particular point source weights in the resulting diffraction pattern is shown by the Gaussian envelope in black. As can be seen different point sources are at different height wherefore the diffraction patterns of different point sources are shifted upwards or downwards. Then by taking the weighted sum of all these diffraction patterns will result in a blurring of fringes.

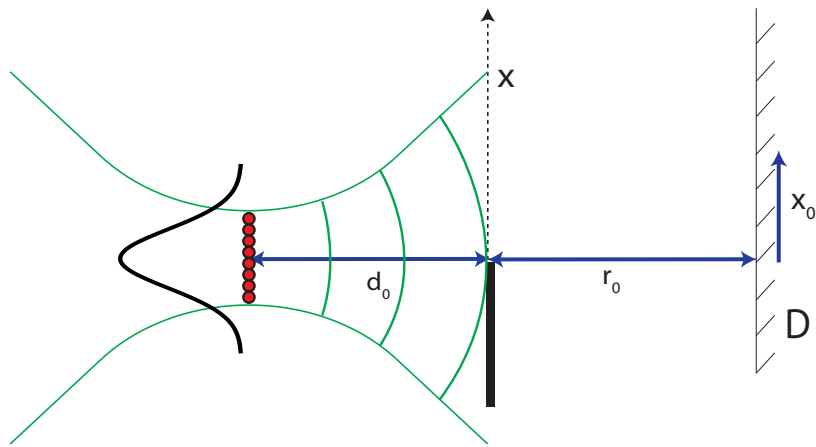


Figure 34: The diffraction geometry of the electron beam build up of subbeams indicated by red dots. These subbeams have a gaussian envelope over them indicating the weight of each subbeam.

In reality however, point sources are not encountered and Gaussian beams need to be used. The idea behind the method to determine the quality of the electron beam using Fresnel diffraction is the same as the method just mentioned. However, here the beam is thought of being built up of Gaussian beams, where the width of each beam is L_x as defined in equation (5.1). By building up the electron beam in this way, one would have an equivalent geometry as in Figure 34 where now the red dots indicate the Gaussian subbeams.

The smaller L_x (compared to σ_x), the less coherent the beam, the more there is a blurring of fringes. At a certain point all the fringes are blurred out. It is at this point that no information of the quality of the electron beam could be extracted from the diffraction pattern anymore.

The same kind of analysis has been done by Clemens Rammeloo [19] for the UCP electron beam. However, Rammeloo also envisioned the electron beam entirely consisting of point sources. The description of Rammeloo is almost right, the only adaption made here is that the point source emitters in his description are replaced by Gaussian beam emitters which have a finite waist. If however, the coherence length L_x , and therefore the width of the subbeams, is so small that the Rayleigh length of these subbeams is small compared to d_0 and r_0 , the approximation of the Gaussian beams by point sources is right. Clemens showed that in his setup, with the rms beam size equal to 100 μm and a coherence length of 20 nm no Fresnel fringes were detected. A coherence length of 20nm allowed him to describe the beam in point sources since the Rayleigh length is about 1000 times smaller than d_0 in his setup. Figure 12b however shows that with a Rayleigh length that is 500 times smaller than d_0 and r_0 , the fringe spacing in the point source Fresnel diffraction pattern is indeed equal to the point source pattern, but the intensity of the Guassain beam diffraction is slightly smaller. So there is some additional influence of the Gaussian beam, but since the real information is in the fringes and there is just a slight decrease in intensity of the fringes, his description of point sources was allowed.

In his thesis Rammeloo illustrated the blurring effect clearly in Figure 35 shown below from his thesis.

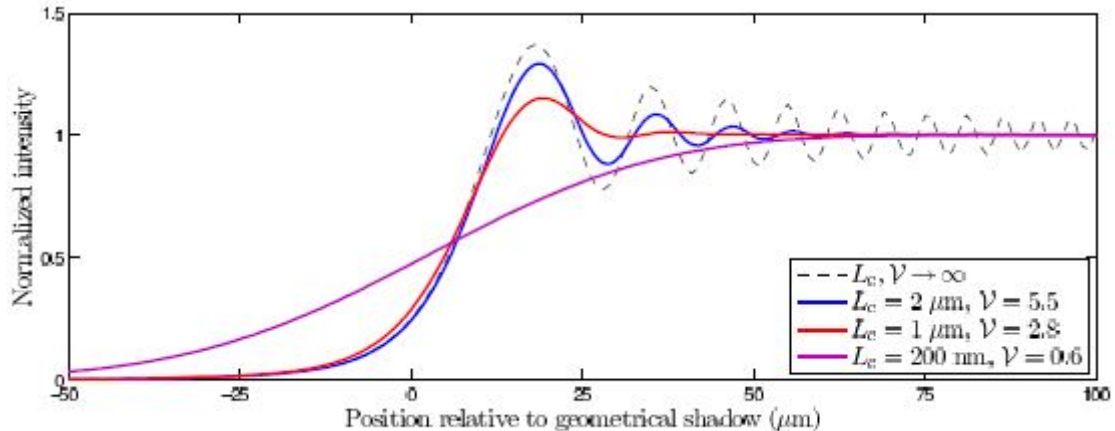


Figure 35: Blurring effect due to the different point sources/Gaussian subbeams where from the beam is built up. The higher the degree of coherence, the higher the coherence length, the lesser the blurring [19]

In this figure the blurring is shown as function of the coherence length L_c in his thesis. In this thesis this is called L_x . Next to the coherence length he defined a visibility V , which is a measure for the degree to which a fringe is visible. What can bee seen is that the visibility decreases with decreasing coherence length and that at a certain point no fringes are visible anymore. It is at that point that this method is not able to give accurate information about the degree of coherence of the beam. It turned out that the coherence of the UCP electron beam was too low to see these Fresnel diffraction fringes and therefore this method could not be applied.

However a slit could be used to enhance the visibility of Fresnel diffraction fringes by the

following reasoning. If a slit is placed somewhere inside the beam line of the UCP setup that cuts a certain amount of the beam, the convolution of the intensity pattern does not run over the entire distance of the Gauss anymore. Therefore the resulting diffraction pattern is an incoherent sum of lesser Gaussian subbeams which enhances the visibility of the final diffraction pattern. By placing a slit in the setup σ_x in equation (5.1) is reduced while L_x is constant.

The only thing that has to be taken into account in this slit geometry is that the slit itself also shows diffraction. For the major part of the electron beam to not be influenced by this diffraction on the slit, Fresnel diffraction has to occur instead of Fraunhofer diffraction since in Fraunhofer diffraction, the diffraction influences the entire beam width while Fresnel diffraction only influences the beam at the edges of the slit. The diffraction range of the edges of these slits needs to be smaller than, as a rough measure, say 20% of the remaining beam size for these slits to not influence the center of the beam. For the slit to show Fresnel diffraction $\frac{D}{\sqrt{\lambda d_{drift}}}$ has to be larger than 1 as explained in section 2, where D is the width of the slit and d_{drift} is the distance between the slit and the place where the diffraction is measured. Then the range where on diffraction of the edges takes place can be calculated using equation (2.39). So the center to not notice the diffraction effects the beam size needs to be $\frac{\text{equation (2.39)}}{0.2}$.

So by the method above, the degree of coherence can be determined where the measure of coherence is the blurring of the Fresnel diffraction fringes. In the UCP setup the degree of coherence was approximately 10^{-4} which turned out to be too small. In literature it has been shown that Fresnel fringes are measured when the degree of coherence, C_x , is approximately 10^{-2} [20]. The minimal degree of coherence where from diffraction fringes are visible is determined by the setup used. For example, the spacing between the first and the second fringe in the point source diffraction scales as $\frac{r_0}{\sqrt{d_0}}$ if $r_0 \gg d_0$ as can easily be derived from equation (2.18) whereas the shifting of a the diffraction pattern due to a point source on a height x_s scales as $\frac{r_0}{d_0}$. The first fringes actually only gets blurred if the shifting of the pattern of a point source is larger than the fringe spacing between the first and second fringe. Since the spacing depends on $\frac{1}{\sqrt{d_0}}$ and the shifting on $\frac{1}{d_0}$, the visibility increases if d_0 is larger. However, the just mentioned approximation of the fringe spacing might not be valid anymore, but still there is a less strong fall off than $\frac{1}{d_0}$ in the shifting of the pattern which makes it beneficial to enlarge d_0 . The practical problem however is that there is a limited length of the beam line. Next to increasing d_0 , λ could be increased since the fringe spacing scales as $\sqrt{\lambda}$ while the shifting is independent of λ . Increasing λ is equivalent to decreasing the energy of the beam.

In this thesis no more work has been done on this subject. In future investigations further work could be done on this subject and better quantizations could be made to set up criterion that the UCP beam line setup has to fulfill in order to see Fresnel diffraction fringes.

6 Conclusion

The goal of this thesis was to develop a theory of Fresnel diffraction to serve as a basis to determine the coherence of an electron beam. As mentioned in the introduction, lots of experiments involve electron beam diffraction on samples and for these experiments to work, the coherence length of an electron beam must be larger than the typical length of samples. For this reason it is useful to determine the coherence of such a beam. The coherence of an electron beam using Fresnel diffraction has already been done by N. De Jonge. N. De Jonge dealt with a source size of 2.1nm and therefore was allowed to use the theory of point source Fresnel diffraction. When dealing with larger beam sizes the theory of point source diffraction becomes less realistic and the theory of a Gaussian beam has to be applied.

In this thesis the theory of Fresnel diffraction on a semi-infinite opaque screen of a plane wave and a point source has been reviewed. These two beam profiles are ideal and not encountered in nature. A beam profile that is encountered in nature is the Gaussian beam. The Gaussian beam perfectly connects the point source to the plane wave. Up till before this thesis the theory of Fresnel diffraction of a Gaussian beam was not known by the author. In this thesis this new theory on Fresnel diffraction of a Gaussian beam has been developed. It turned out that the Fresnel diffraction pattern of a Gaussian is the product of a Gaussian amplitude fall-off term and a diffraction form factor. And where the beam profile of the Gaussian beam converged to the plane wave and point source limit, it has also been shown that the Fresnel diffraction pattern also converges perfectly to that of a plane wave and a point source.

The reviewed theory of plane wave diffraction and point source diffraction as well as Gaussian beam diffraction have been tested in an experiment. In these experiments Fresnel diffraction patterns have been measured that qualitatively confirm the theory has been developed. Some deviations have been noticed in the fit parameters that could (partially) be explained by the way the experiment has been setup. It has also been shown that the location of the center of the Gaussian beam compared to the edge of the semi-infinite screen becomes less important as the beam waist, or rather the Rayleigh length, increases. Next to this it has been verified that the fringe spacing depends on the geometry chosen. In doing these experiments it has been noticed that the use and position of lenses in the experimental setup influences the Fresnel diffraction pattern.

The theory developed could be used to determine the quality of an electron beam by measuring Fresnel diffraction of an electron beam. Where for a fully coherent beam the Fresnel diffraction pattern consists of clearly visible fringes, the Fresnel diffraction pattern of a partially coherent electron beam shows blurred fringes. This blurring is due to the fact that a partially coherent beam is being thought of as incoherently built up of coherent beams. Therefore the diffraction patterns of these coherent beams also need to be added incoherently. The degree to which fringes are still visible is a measure of the coherence.

6.1 Outlook

In the future the theory of Fresnel diffraction could be used in the UCP setup, as well as in other setups using electron beams, to determine the coherence of an electron beam. At this time, the coherence of the UCP setup seems to be too low to show any Fresnel diffraction fringes. However, adjustments in the setup can be made for the fringes to be better visible. The feasibility of this method has not been quantified at this time. This certainly is an interesting aspect for following research. To detect Fresnel diffraction fringes a number of aspects need to be taken into account, which are for example the energy spread of the

electron beam. This influences the wavelength and therefore the diffraction pattern. More practical aspects that need to be taken into account are the following:

- Spread in angle distribution of electron beam
- Since the electron beam is extracted from a magneto optical trap (MOT) in the UCP, the motion in the longitudinal direction as transversal direction of the MOT have to be considered.
- In the UCP setup, solonoid lenses are used to focus the beam size. Possibly there is an optimal spot size to see the Fresnel diffraction fringes that could be made solonoid lenses in the UCP setup.
- The use of a slit in the beam line to increase the degree of coherence.
- The resolution of the camera that detects the electrons. When using an MCP, the resolution could also be limited by the MCP instead of the camera.

7 References

- [1] K. Schoots N. de Jonge, Y. Lamy and T.H. Oosterkamp. High brightness electron beam from a multi-walled carbon nanotube. *Nature*, Vol. 420, No. 10:393–395, 2002.
- [2] Brent L Nannenga and Tamir Gonen. Femtosecond electron diffraction: heralding the era of atomically resolved dynamics. *Reoprts Prog. Phys.*, 74:096101, 2011.
- [3] P.L.E.M. Pasmans. *Ultrafast electron diffraction, an investigation of fundamental limits*. PhD thesis, University of Technology Eindhoven, 19-06-2014.
- [4] M. Lebeau et al. Standardless atom counting in scanning transmission electron microscopy. *Nano Lett.*, 10:4405–4408, 2010.
- [5] M. Takahashi K. Takayanagi, Y. Tanishiro and S. Takahashi. Structural analysis of si(111)-7x7 by uhv-transmission electron diffraction and microscopy. *J. Vac. Sci. Technol. A*, 3:1502, 1985.
- [6] G. Sciaiani and R.J.D. Miller. Protein structure determination by microed. *Current Opinion in Structural Biology*, 27:24–31, 2014.
- [7] F. Krausz, G. Korn, P. Corkum, I.A. Walmsley. *Ultrafast Optics IV*. Springer, 2014. p. 419-437.
- [8] E. Hecht. *Optics*. Pearson, 4th eddition edition, 2004.
- [9] P.W. Hawkes, E. Kasper. *Wave Optics, 3th edition*, volume 3. Academic Press, 1994.
- [10] M.W. van Mourik. Ultrafast electron diffraction using an ultracold source. *Eindhoven University of Technology*, 2012.
- [11] A.E. Siegman. *LASERS*. University Science Books, 1986.
- [12] Joerg Enderlein Francesco Pampaloni. Gaussian, hermite-gaussian, and laguerre-gaussian beams: A primer, 2004, Oct 4th. URL <http://arxiv.org/abs/physics/0410021>. 24-06-2015.
- [13] H. Kogelnik and T. Li. Laser beams and resonators. *Applied Optics*, Vol. 5, No. 10:1550–1554, 1966.
- [14] JDSU. Helium-neon laser heads, 1100 series, 2010, October. URL http://www.jdsu.com/ProductLiterature/hnlh1100_ds_cl_ae.pdf. 24-06-2015.
- [15] Fly Point Grey. Flea 2 technical reference manual, 2011, June 10th. URL <http://www.ptgrey.com/flea2-08-mp-mono-firewire-1394b-sony-icx204-camera>. 24-06-2015.
- [16] D.J. Bakker E.J.D. Vredenbregt O.J. Luiten W.J. Engelen, M.A. van der Heijden. High-coherence electron bunches produced by femtosecond photoionization. *Nataure Communications*, Vol. 4, No. 1693, 2013.
- [17] M. Reiser. *Theory and Design of Charged Particle Beams*. Wiley-VCH, 2008.
- [18] C.C. Gerry and P.L. Knight. *Introductory quantum optics*. Cambridge university press, third printing edition, 2005.
- [19] C.V. Rammeloo. Master thesis: Measuring the electron beam quality of an ultracold plasma setup. *Eindhoven University of Technology*, 2012.
- [20] W. Qian J.C.H. Spence and M.P. Silverman. Electron source brightness and degeneracy from fresnel fringes in field emission point projection microscopy. *Journal of Vacuum Science and Technology A: Vacuum, Surfaces and Films*, Vol. 12:542, 1994.

A Derivation of relation between errorfunction and fresnel-function

To be proven:

$$\operatorname{erf}[x] = (1-i)F\left[\frac{2}{\sqrt{\pi}(1-i)}x\right] \quad (\text{A.1})$$

Start by noting that $F(z) = \int_0^z \exp\left(\frac{i\pi}{2}t^2\right) dt$. This means that

$$F\left[\frac{2}{\sqrt{\pi}(1-i)}x\right] = \int_0^{\frac{2}{\sqrt{\pi}(1-i)}x} \exp\left(\frac{i\pi}{2}t^2\right) dt. \quad (\text{A.2})$$

Now lets introduce $\kappa = \frac{\sqrt{\pi}(1-i)}{2}t$. This has the effect of changing the upper integration boundary in equation (A.2) to x and leaves the lower integration boundary unchanged.

Next to that it gives that

$$t = \frac{2}{\sqrt{\pi}(1-i)}\kappa \quad (\text{A.3})$$

$$\Rightarrow t^2 = \frac{4}{\pi(1-i)^2}\kappa^2 = \frac{4}{-2i\pi}\kappa^2 = -\frac{2}{i\pi}\kappa^2 \quad (\text{A.4a})$$

$$\Rightarrow dt = \frac{2}{\sqrt{\pi}(1-i)} d\kappa \quad (\text{A.4b})$$

Substitution of the new boundaries and equations (A.4a) and (A.4b) in equation (A.2) gives

$$F\left[\frac{2}{\sqrt{\pi}(1-i)}x\right] = \frac{2}{\sqrt{\pi}(1-i)} \int_0^x \exp(-\kappa^2) d\kappa, \quad (\text{A.5})$$

which means that

$$\operatorname{erf}[x] = \frac{2}{\sqrt{\pi}} \exp(-\kappa^2) d\kappa = (1-i)F\left[\frac{2}{\sqrt{\pi}(1-i)}x\right]. \quad (\text{A.6})$$

So equation (A.1) is valid. \square

B Derivation expressions Γ and ϕ

B.1 derivation of simplified relation for γ

In this part of the appendix it will be shown that γ could be written as $\frac{1}{\lambda^2}\pi\left[-\frac{i}{\mu} + \frac{1}{i\rho+\pi\sigma^2}\right]$. Start by using the definition of γ from equation (2.31), using relations (2.36) and using the relations stated in (2.27b) and (2.27b) γ could be written as

$$\begin{aligned} \gamma &= \frac{1}{\lambda^2} \left[\frac{1}{\sigma^2 \left(1 + \frac{\rho^2}{\pi^2 \sigma^4}\right)} - i\pi \left\{ \frac{1}{\rho \left(1 + \frac{\pi^2 \sigma^4}{\rho^2}\right)} + \frac{1}{\mu} \right\} \right] \Rightarrow \\ \lambda^2 \gamma &= \frac{1}{\sigma^2 \left(1 + \frac{\rho^2}{\pi^2 \sigma^4}\right)} + \pi \frac{1}{i\rho \left(1 + \frac{\pi^2 \sigma^4}{\rho^2}\right)} - \frac{i\pi}{\mu}. \end{aligned}$$

Factoring the first two terms gives

$$\lambda^2 \gamma = \frac{i\rho \left(1 + \frac{\pi^2 \sigma^4}{\rho^2}\right) + \sigma^2 \left(1 + \frac{\rho^2}{\pi^2 \sigma^4}\right)}{i\sigma^2 \rho \left(1 + \frac{\rho^2}{\pi^2 \sigma^4}\right) \left(1 + \frac{\pi^2 \sigma^4}{\rho^2}\right)} - \frac{i\pi}{\mu}$$

writing this out leaves

$$\begin{aligned} \lambda^2 \gamma &= \frac{i\rho + \frac{\rho^2}{\pi^2 \sigma^2} + \pi \sigma^2 + \frac{i\pi^2 \sigma^4}{\rho}}{\frac{i\rho^3}{\pi^2 \sigma^2} + 2i\rho \sigma^2 + \frac{i\pi^2 \sigma^6}{\rho}} - \frac{i\pi}{\mu} = \frac{i\rho^2 \pi^2 \sigma^2 + i\pi^4 \sigma^6 + \rho \pi^3 \sigma^3 + \pi \rho^3}{2i\sigma^4 \pi^2 \rho + i\rho^4 + i\pi^4 \sigma^8} - \frac{i\pi}{\mu} \\ &= \frac{i\rho^2 \pi^2 \sigma^2 + i\pi^4 \sigma^6 + \rho \pi^3 \sigma^3 + \pi \rho^3}{\frac{1}{\pi} (i\rho + \pi \sigma^2) (i\rho^2 \pi^2 \sigma^2 + i\pi^4 \sigma^6 + \rho \pi^3 \sigma^3 + \pi \rho^3)} - \frac{i\pi}{\mu} = \frac{\pi}{i\rho + \pi \sigma^2} - \frac{i\pi}{\mu}. \end{aligned}$$

So indeed

$$\gamma = \frac{1}{\lambda^2} \pi \left(\frac{1}{i\rho + \pi \sigma^2} - \frac{i\pi}{\mu} \right). \quad (\text{B.1})$$

B.2 deriving the expression for $\sqrt{\frac{2}{\pi} \frac{\beta}{2\sqrt{\gamma}}}$

using the expression derived for γ in equation (B.1) and the expression for β in equation (2.32) it yields that

$$\frac{\beta}{2\sqrt{\gamma}} = -\frac{i\sqrt{\pi}}{\lambda \mu \sqrt{\frac{1}{i\rho + \pi \sigma^2} - \frac{i\pi}{\mu}}}. \quad (\text{B.2})$$

To futher investigate this expression, $\zeta = \frac{1}{i\rho + \pi \sigma^2} - \frac{i\pi}{\mu}$, will be written in polar coordinates.

$$\begin{aligned} \frac{1}{i\rho + \pi \sigma^2} - \frac{i\pi}{\mu} &= \frac{\rho - i\pi \sigma^2 + \mu}{\mu (i\rho + \pi \sigma^2)} = \frac{\rho - i\pi \sigma^2 + \mu}{\mu (i\rho + \pi \sigma^2)} \cdot \frac{-i\rho + \pi \sigma^2}{-i\rho + \pi \sigma^2} \\ &= \frac{-i\rho - \pi \sigma^2 \rho - i\mu \rho + \pi \sigma^2 \rho - i\pi^2 \sigma^4 + \mu \pi \sigma^2}{\mu (\rho^2 + \pi^2 \sigma^4)} \\ &= \frac{1}{\mu (\rho^2 + \pi^2 \sigma^4)} [\mu \pi \sigma^2 - i(\rho^2 + \mu \rho + \pi^2 \sigma^4)]. \end{aligned}$$

From this the absolute value and the argument could be determined. First, the absolute value will be determined, second the argument will be determined.

$$\begin{aligned} |\zeta| &= \frac{1}{\mu (\rho^2 + \pi^2 \sigma^4)} \sqrt{\mu^2 \pi^2 \sigma^2 + (\rho^2 + \mu \rho + \pi^2 \sigma^4)^2} \\ &= \frac{1}{\mu (\rho^2 + \pi^2 \sigma^4)} \sqrt{\mu^2 \pi^2 \sigma^2 + \rho^4 + 2\mu \rho^3 + 2\pi^2 \sigma^4 \rho^2 + \mu^2 \rho^2 + 2\mu \rho \pi^2 \sigma^4 + \pi^4 \sigma^8} \\ &= \frac{1}{\mu (\rho^2 + \pi^2 \sigma^4)} \sqrt{\rho^2 + \pi^2 \sigma^4} \sqrt{(\mu + \rho)^2 + \pi^2 \sigma^4} = \frac{1}{\mu} \sqrt{\frac{(\mu + \rho)^2 + \pi^2 \sigma^4}{\rho^2 + \pi^2 \sigma^4}}, \end{aligned}$$

call this quantity κ , so

$$\kappa = \frac{1}{\mu} \sqrt{\frac{(\mu + \rho)^2 + \pi^2 \sigma^4}{\rho^2 + \pi^2 \sigma^4}}. \quad (\text{B.3})$$

Lets now consider the argument of ζ and call this argument ϕ . Then

$$\phi = \arctan \left[-\frac{\rho^2 + \mu \rho + \pi^2 \sigma^4}{\mu \pi \sigma^2} \right]. \quad (\text{B.4})$$

So written in polar coordinates,

$$\zeta = \kappa \exp(i\phi + 2i\pi m), \quad (\text{B.5})$$

where m is an integer.

Now the expression for ζ in polar coordinates is known, it could be substituted in equation (B.2) and this equation could then also be expressed in polar coordinates. So

$$\frac{\beta}{2\sqrt{\gamma}} = -\frac{i\sqrt{\pi}}{\lambda\mu\sqrt{\kappa}} \exp\left(-\frac{i}{2}\phi + i\pi m\right)$$

This yields two different solutions, one for $m = 0$ and one for $m = 1$. The only difference between these two cases is a “-” sign, so this means

$$\frac{\beta}{2\sqrt{\gamma}} = \pm \frac{i\sqrt{\pi}}{\lambda\mu\sqrt{\kappa}} \exp\left(-\frac{i}{2}\phi\right) = \pm \frac{\sqrt{\pi}}{\lambda\sqrt{\Gamma'}} \exp\left(-\frac{i}{2}\phi\right) \exp\left(-\frac{i\pi}{2}\right) = \pm \frac{\sqrt{\pi}}{\lambda\sqrt{\Gamma'}} \exp\left(-\frac{i}{2}[\phi + \pi]\right),$$

with

$$\Gamma' = \mu \sqrt{\frac{(\mu + \rho)^2 + \pi^2\sigma^4}{\rho^2 + \pi^2\sigma^4}}. \quad (\text{B.6})$$

Eventually the argument of the fresnelfunction is $\frac{2}{\sqrt{\pi}(1-i)} \frac{\beta}{2\sqrt{\gamma}} = \sqrt{\frac{2}{\pi}} \frac{\beta}{2\sqrt{\gamma}} \exp\left(\frac{i\pi}{4}\right)$. By using what has just been derived, this could be written entirely in polar coordinates yielding for the argument of the fresnelfunction

$$\frac{2}{\sqrt{\pi}(1-i)} \frac{\beta}{2\sqrt{\gamma}} = \pm \frac{1}{\lambda\sqrt{\Gamma}} \exp\left(-\frac{i}{2}[\phi + \frac{\pi}{2}]\right). \quad (\text{B.7})$$

With

$$\Gamma = \frac{\mu}{2} \sqrt{\frac{(\mu + \rho)^2 + \pi^2\sigma^4}{\rho^2 + \pi^2\sigma^4}}. \quad (\text{B.8})$$

C Derivation width gaussian beam after diffraction

In this part of the appendix the derivation of the broadening of the gaussian beam caused by diffraction will be mathematically derived. The gaussian fall off term equals $\exp\left(\frac{\beta^2}{4} \left[\frac{1}{\gamma} + \frac{1}{\gamma^*}\right] x_0^2\right)$ as is stated in section 2.5.3.

$$\exp\left(\frac{\beta^2}{4} \left[\frac{1}{\gamma} + \frac{1}{\gamma^*}\right] x_0^2\right) = \exp \chi, \quad \text{with} \quad \chi = \frac{\beta^2}{4} \left[\frac{1}{\gamma} + \frac{1}{\gamma^*}\right] x_0^2 \quad (\text{C.1})$$

Using the definitions for γ and β in equations (2.31) and (2.32), this could be rewritten as

$$\chi = -\frac{k^2 x_0^2}{4r_0^2} \left[\frac{\frac{2}{w^2}}{\frac{1}{w^4} + \frac{k^2}{4r_0^2 R^2} (R + r_0)^2} \right] = \frac{4r_0^2}{k^2 w^4} \left[1 + \frac{k^2 w^4}{4r_0^2} \left(\frac{R + r_0}{R} \right)^2 \right] \frac{2x_0^2}{w^2} \quad (\text{C.2})$$

$$= \frac{2x_0^2}{\sigma_{rms}^2} \quad (\text{C.3})$$

So

$$\begin{aligned}\sigma_{rms}^2 &= w^2 \left[\left(\frac{2r_0}{kw^2} \right)^2 \left\{ 1 + \left(\frac{kw^2}{2r_0} \right)^2 \left(\frac{R+r_0}{R} \right)^2 \right\} \right] \\ &= w^2 \left[\left(\frac{2r_0}{kw^2} \right)^2 + \left(\frac{R+r_0}{R} \right)^2 \right].\end{aligned}$$

So σ_{rms} equals $w(z)$ with a scaling factor. Using equations (2.27a), (2.27b) and (2.36) this could be rewritten as

$$\sigma_{rms}^2 = w^2 \left[\left(\frac{\mu}{\pi\sigma^2 \left[1 + \left(\frac{\rho}{\pi\sigma^2} \right)^2 \right]} \right)^2 + \left(1 + \frac{\mu}{\rho \left[1 + \left(\frac{\pi\sigma^2}{\rho} \right)^2 \right]} \right)^2 \right]$$

Expanding the powders gives

$$\sigma_{rms}^2 = w^2 \left[1 + \frac{\mu^2}{\rho^2 \left(\frac{\pi^2\sigma^4}{\rho^2} + 1 \right)^2} + \frac{\mu^2}{\pi^2\sigma^4 \left(\frac{\rho^2}{\pi^2\sigma^4} + 1 \right)^2} + \frac{2\mu}{\rho \left(\frac{\pi^2\sigma^4}{\rho^2} + 1 \right)} \right]$$

Now giving all terms except the first one the same denominator leaves

$$\begin{aligned}\sigma_{rms}^2 &= w^2 \left[1 + \frac{\frac{\mu^2\rho^4}{\pi^2\sigma^4} + \frac{\pi^4\mu^2\sigma^8}{\rho^2} + 3\mu^2\rho^2 + 3\pi^2\mu^2\sigma^4 + \frac{2\mu\rho^5}{\pi^2\sigma^4} + 6\mu\rho^3 + \frac{2\pi^4\mu\sigma^8}{\rho} + 6\pi^2\mu\rho\sigma^4}{\frac{\rho^6}{\pi^2\sigma^4} + 4\rho^4 + \frac{\pi^6\sigma^{12}}{\rho^2} + 6\pi^2\rho^2\sigma^4 + 4\pi^4\sigma^8} \right] \\ &= w^2 \left[1 + \frac{\frac{(\rho^2+\pi^2\sigma^4)^3}{\pi^2\rho^2\sigma^4} \mu (\mu + 2\rho)}{\frac{(\rho^2+\pi^2\sigma^4)^3}{\pi^2\rho^2\sigma^4} (\rho^2 + \pi^2\sigma^4)} \right] \\ &= w^2 \left[1 + \frac{\mu (\mu + 2\rho)}{\rho^2 + \pi^2\sigma^4} \right]\end{aligned}$$

So

$$\sigma_{rms}^2 = w^2 \left[1 + \frac{\mu (\mu + 2\rho)}{\rho^2 + \pi^2\sigma^4} \right] \quad (\text{C.4})$$

To arrive at the σ_{rms}^2 as in equation (2.40), w is written in terms as in (2.27a) with equations (2.36) replaced. This gives

$$\sigma_{rms}^2 = \lambda^2 \sigma^2 \left(1 + \frac{\rho^2}{\pi^2\sigma^4} \right) \left(1 + \frac{\mu(\mu + 2\rho)}{\rho^2 + \pi^2\sigma^4} \right) \quad (\text{C.5})$$

Working out the multiplication and giving each term the same denominator leaves

$$\begin{aligned}\sigma_{rms}^2 &= \lambda^2 \left[\frac{\mu^2\rho^2 + \pi^2\mu^2\sigma^4 + 2\mu\rho^3 + 2\pi^2\mu\rho\sigma^4 + \pi^2\sigma^4 (\rho^2 + \pi^2\sigma^4) + \rho^2 (\rho^2 + \pi^2\sigma^4)}{\pi^2\sigma^2 (\rho^2 + \pi^2\sigma^4)} \right] \\ &= \lambda^2 \left[\frac{\left(\frac{(\mu+\rho)^2}{\pi^2\sigma^2} + \sigma^2 \right) \pi^2\sigma^2 (\pi^2 + \pi^2\sigma^4)}{\pi^2\sigma^2 (\pi^2 + \pi^2\sigma^4)} \right] \\ &= \lambda^2 \left[\sigma^2 + \frac{(\mu + \rho)^2}{\pi\sigma^2} \right]\end{aligned}$$

So, as is stated in section 2.5.3

$$\sigma_{rms}^2 = \lambda^2 \left[\sigma^2 + \frac{(\mu + \rho)^2}{\pi\sigma^2} \right] \quad (\text{C.6})$$

By substituting equation 2.36 and the relation between S and x_s in equation (2.42) the dimensionful equation describing the Gaussian beam diffraction could be derived to be as

$$|\psi(x_0, y_0, z=r_0+d_0)|^2 = \frac{1}{2} \exp \left(-\frac{(x_0 - x_s)^2}{(d_0 + r_0)^2 \frac{\lambda^2}{\pi^2 w_0^2} + w_0^2} \right) \\ \left[1 + (1 - i) \left(F \left[\left(\sqrt{\frac{2}{\lambda r_0}} \exp \left(\frac{i}{2} \left[\Phi + \frac{\pi}{2} \right] \right) \sqrt{\frac{1}{T}} x_s \right. \right. \right. \right. \\ \left. \left. \left. \left. + \sqrt{\frac{2}{\lambda r_0}} \exp \left(-\frac{i}{2} \left[\Phi + \frac{\pi}{2} \right] \right) \sqrt{T} [x_0 - x_s] \right] \right] \right) \right] \quad (\text{C.7})$$

with

$$T = \sqrt{\frac{\frac{\pi^2 w_0^4}{\lambda^2} + d_0^2}{\frac{\pi^2 w_0^4}{\lambda^2} + (d_0 + r_0)^2}} \quad (\text{C.8})$$

$$\Phi = \arctan \left(-\frac{\left(\frac{\pi^2 w_0^4}{\lambda^2} + d_0 r_0 + d_0^2 \right)}{r_0 \frac{\pi w_0^2}{\lambda}} \right)$$

From this it could be seen the importance of d_0 always is relative to the Rayleigh length, $z_R (= \frac{\pi w_0^2}{\lambda})$.

D Beam size measurement

In section 4.1 data on the beam size has been presented. This data was measured by shining the beam on millimeter paper and these measurements are shown by the pictures below. The left picture is the beam size at 50 cm behind the last lens, the middle picture is at 212 cm behind the last lens and the right picture is at 482 cm behind this lens.

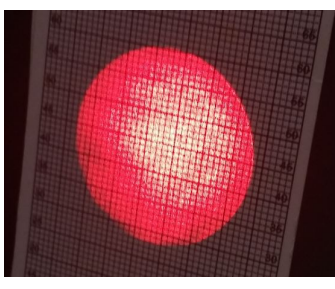


Figure 36: Beam size 50 cm behind the last lens

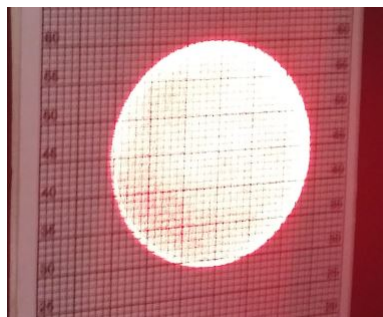


Figure 37: Beam size 212 cm behind the last lens

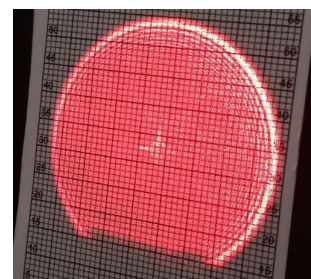


Figure 38: Beam size 482 cm behind the last lens

E Camera angle influence

Here the two measured diffraction patterns with a difference of angle position of the camera to the propagation direction of the beam are presented.

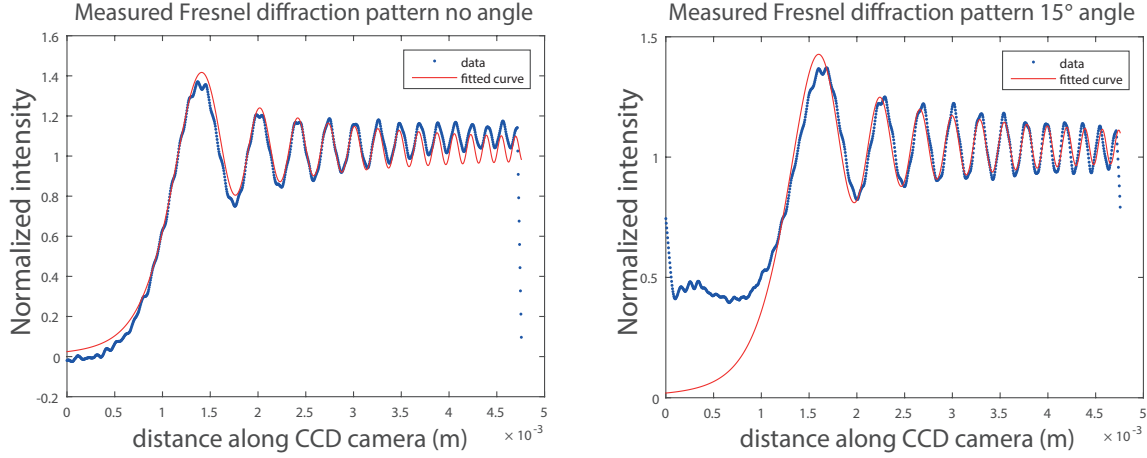


Figure 39: The left figure is the pattern where the camera seems to be positioned perpendicular to the propagation direction. The right figure is where the camera is positioned 15 degrees as compared to the left figure.

The data in the figures are fitted with equation (4.1) multiplied by I_0 and x_0 replaced by $x_0 - x_v$. From the left fit a r_0 value of $(91.9 \pm 0.2)\text{cm}$ is measured while from the right fit a value of $(102 \pm 6.09 \cdot 10^{-3})\text{cm}$ is measured. So setting the camera under 15 degrees results in a difference of 10 centimeter in r_0 for this particular setup.

In the right figure the experimental data seems to reach a lower boundary. This is due to the method by which this figure is analyzed in Matlab. As mentioned in section 4 the background image is subtracted from the diffraction image where after the average of the background image is added again. Since by turning the camera some the light intensity of this background is not uniform over the entire CCD. In the region before the first fringe the intensity is lower than in the fringe region. Therefore subtracting the background image and adding its average results in a artificial intensity before the first fringe.

F Fit parameters of section 4

Fit parameters of plane wave diffraction

Table 10: Fit parameters of figure 26

	x_v (mm)	x_s (mm)	w_0 (mm)	r_0 (cm)
Figure 26a	0.351	1.653	3.42	48.24
68% \pm Figure 26a	0.001	0.002	0.01	0.03
Figure 26b	0.770	1.25	3.30	48.5
68% \pm Figure 26b	0.001	0.01	0.02	0.1
Figure 26c	1.197	0.92	3.10	49.1
68% \pm Figure 26c	0.001	0.01	0.03	0.1